NASA Contractor Report 195450

A 75 Watt, 59 to 64 GHz Space TWT

Helen Limburg, Diego Zamora, Jon Davis, and Ivo Tammaru
Hughes Aircraft Co.
Torrance, California

April 1995

Prepared for
Lewis Research Center
Under Contract NAS3–25090

National Aeronautics and
Space Administration

TABLE OF CONTENTS

LIST OF ILLUSTRATIONS

LIST OF ILLUSTRATIONS (CONTINUED)

LIST OF TABLES

1.0 SUMMARY

This report describes the further development of a 75 watt, 60 GHz traveling-wave tube for inter-satellite communications to meet the requirements of NAS3-25090. This TWT, designated Hughes model 961HA, extends the performance of V-band space TWTs to higher power and bandwidth than previously achieved. The objective frequency band was 59 to 64 GHz, with a minimum tube gain of 35 dB. The objective overall efficiency at saturation was 40 percent. Sixty watts minimum and 70 watts average CW output power across the frequency band of 59 to 64 GHz was achieved. The average overall efficiency was 28%. A lossy monel output coupler was used which substantially degraded both rf output power and overall efficiency. The TWT is packaged consistent with the end requirement of conduction cooling for satellite installation and weighs only 5.9 kG(13 lb).

The 961HA TWT uses a coupled-cavity interaction circuit with periodic permanent magnet beam focusing to minimize the weight. A refocusing section between the circuit output and the collector is used. A four-stage depressed collector is used to enhance the efficiency. This collector uses 4 axisymmetric isotropic graphite electrodes, the last stage a spike at cathode potential. The electron gun incorporates an M-type cathode with a loading of 2.0 A/cm^2, consistent with a 10 year life requirement. An isolated anode is incorporated as an ion trap and for ease of turn-on. The cathode voltage is −19.3 kV and the cathode current is 74 mA.

The 961HA design is based on an earlier device, the 961H. The 961HA was designed for the same output power, bandwidth and efficiency as the 961H. Changes were made to the RF circuit to enhance the stability, eliminate a second harmonic interaction and extend performance to the full bandwidth. The 961HA program originally required a dual mode operation, a low power 30 W mode, in addition to the 75 watt mode. This was to be achieved by using two anodes. One anode would be used to limit the full cathode current and thus reduce the power for the low mode of operation. Two TWTs were built with the dual anode electron gun. The dual anode design created difficult beam focusing conditions. This requirement was eliminated and the gun was redesigned for optimum focusing in the high power mode. The 961HA mechanical design is similar to the 961H design with further refinements to achieve performance and packaging. The primary difference is that the 961HA collector is conduction cooled to a baseplate, whereas the 961H had a radiation cooled collector. This report includes the details of the design and the test results.

In summary, development of the 961HA TWT has increased the output power and bandwidth of V-band spaceborne TWTs. To achieve the goal of 75 watts minimum output power across the entire band it is recommended that additional effort be focused on developing ruggedized copper output waveguides with good RF matches, to avoid the large RF dissipation in output waveguides of monel.

2.0 INTRODUCTION

The purpose of the contract effort described in this report was to continue the development of a 75-watt CW, 59 to 64 GHz space borne TWT for inter-satellite communications. The objectives were to improve the 961H baseline TWT design to enhance the bandwidth and stability, provide for dual mode operation (a low power mode of 30 W CW), demonstrate CW operation and modify the package to conduction cool the multistage collector of the tube, as well as ruggedize the tube for the launch and space environment. The nominal operating parameters are summarized in Table 1.

TABLE 1. 961HA NOMINAL OPERATING CHARACTERISTICS

RF Characteristics	
Saturated Output Power	60 W minimum
Frequency	59 to 64 GHz
Gain at Saturation	45 dB
Duty Cycle	CW
Electrical Characteristics	
Cathode Voltage	-19.3 kV
Cathode Current	73.8 mA
Body Voltage	0 V
Body Current (with RF)	3.0 mA
Overall Efficiency	24 % minimum
Collector Voltages	
E_{b1}	-14.9 kV
E_{b2}	-16.8 kV
E_{b3}	-18.0 kV
E_{b4}	-19.3 kV
Collector Current (with RF)	
I_{b1}	24.0 mA
I_{b2}	27.0 mA
I_{b3}	19.9 mA
I_{b4}	0.0 mA
Anode Voltage	100 V
Anode Current	0 mA
Filament Voltage	4.75 V
Filament Current	0.77 A
Ion-Pump Voltage	3.0 kV
Ion-Pump Current	0.1 uA
Mechanical Characteristics	
Focusing	PPM
Cooling	Conduction
Weight	5.9 kG (13 lb.)
Dimensions	44.5 cm (17.5 in.) long x 11.4 cm (4.5 in.) wide x 9.7 cm (3.8 in.) high

The combined requirements of high output power, high efficiency and broad bandwidth are a considerable development challenge for a tube in this frequency range. To meet these goals, a coupled-cavity slow-wave structure is employed because of its thermal ruggedness and demonstrated capability to achieve the required power, bandwidth, and efficiency. For high overall efficiency, a velocity taper at the output of the RF circuit enhances the beam-circuit interaction efficiency and a four-stage depressed collector recovers energy from the spent beam. The collector geometry was optimized by NASA. Isotropic graphite electrodes are used to improve collector efficiency by reducing secondary electron emission.

The electron beam is generated by a convergent flow electron gun designed to operate at −19.7 kV. It has an isolated anode capable of switching the beam on and off and providing an ion trap. It uses a low-temperature, type M impregnated cathode operating at a current density of 2.0 A/cm^2 to satisfy the long life requirement, 10 years. Beam focusing is accomplished with a periodic permanent magnet focusing structure using samarium cobalt magnets and an integrally brazed pole piece assembly.

In the course of the program, three tubes were built and tested. The first two tubes did not focus well. The low duty RF data of 961HA S/N 1 showed that the design output power and bandwidth, as well as the efficiency goal was achievable. S/N 1 also demonstrated that the instability present on the preceding design (the 961H) had been effectively eliminated by the changes made to the circuit geometry. This first dual anode tube did not focus well enough to be processed CW. The second dual anode tube also had poor focusing. The VSWR was not as good as S/N 1 and RF data were not taken.

Prior to building S/N 3 the requirement for the low power mode was eliminated. The electron gun and focusing structure were modified accordingly. The RF coupler material was changed from copper to monel for improved mechanical rigidity. In addition S/N 3 was assembled in two halves and then welded in the center. This eliminated the braze operation that degraded the VSWR. S/N 3 achieved excellent focusing. RF output power of 60 watts across the 59 to 64 GHz bandwidth was achieved. The tube was packaged in a conduction cooled baseplate consistent with the end requirement of conduction cooled space operation. Figure 1 is a photograph of S/N 3.

The following sections of this report describe the design details, and performance results of the 961HA traveling-wave tubes.

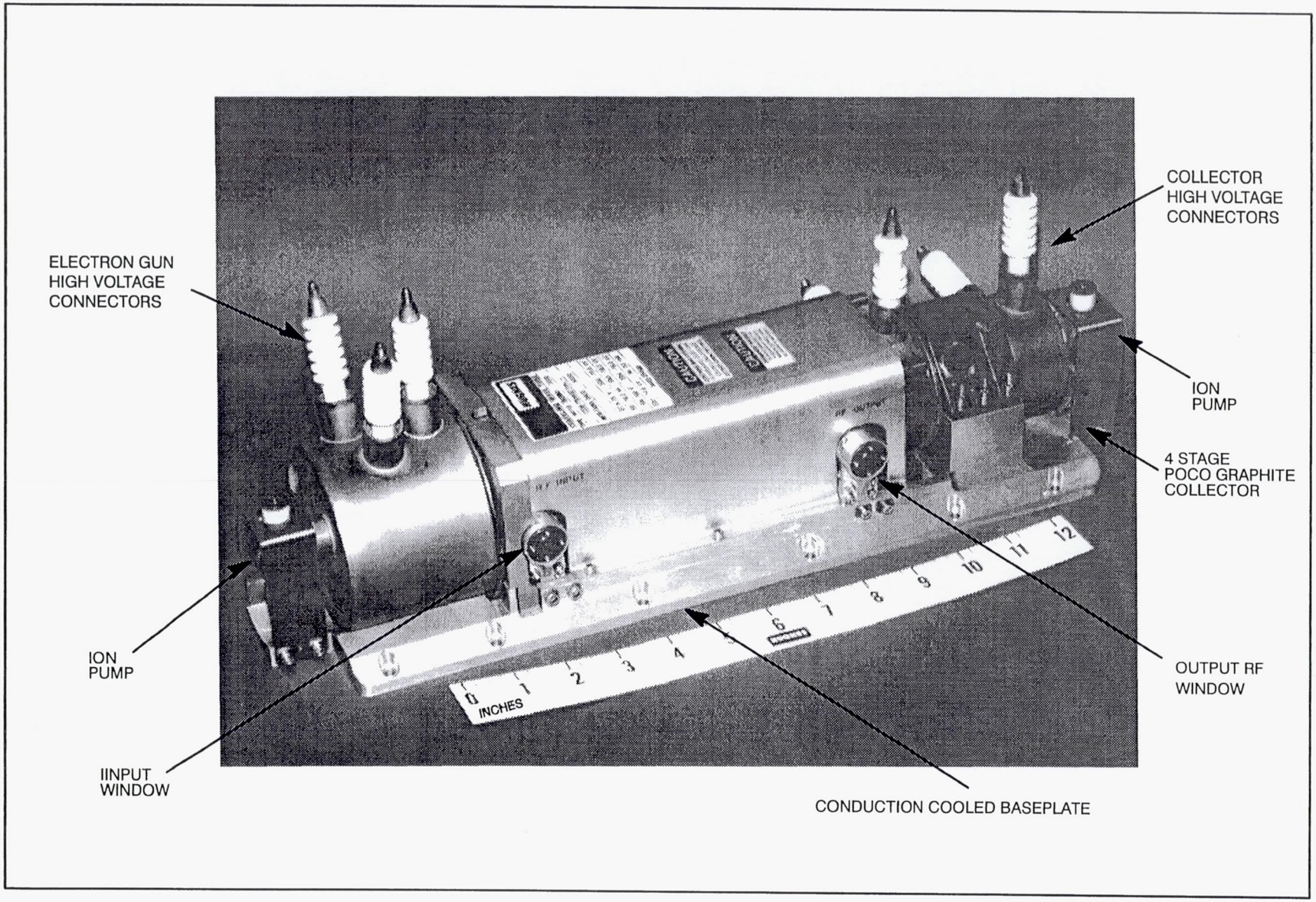

Figure 1. Packaged 961HA TWT.

3.0 TWT DESIGN

3.1 RF CIRCUIT DESIGN

The 961HA RF circuit was based on work performed on the 961H contract. This work is summarized here only as it applied to the final circuit design, the 961HA.

3.1.1 Parametric Analysis

The RF circuit design was initiated with a computer-aided parametric analysis. This is a tradeoff study to optimize often conflicting performance characteristics. Through an iterative process the beam parameters (current, voltage, diameter, and cathode loading) and the RF cavity dimensions are determined consistent with reliable focusing and good beam-RF interaction.

Good focusing of an electron beam requires adequate field strength for sufficient confinement force. In PPM focusing there is also a limitation on the length of the magnetic field period, for beam focusing stability. Greater magnetic field can be obtained with a longer period, but the period is constrained for stability. Therefore, the optimum design is determined by the relationship between the obtainable field and the magnetic period.

The lower the beam voltage the larger the beam hole has to be to maintain good focusing. However as the beam hole becomes larger the interaction efficiency and the performance bandwidth decrease. A low cathode current density, for long life, has a similar adverse effect on efficiency and bandwidth. In addition, a larger cathode size with a larger beam area compression makes it more difficult to achieve a well focused beam. An upper limit of −20 kV beam voltage was established by the specification. This is the upper limit of spaceborne TWT power supplies. The cathode loading was limited to 2.0 A/cm^2 to be consistent with a 10 year life requirement. The results of the tradeoff study are the parameters listed in Table 2.

TABLE 2. CAVITY AND RF INTERACTION PARAMETERS

Cathode Voltage, E_k	−19.7 kV nominal
Cathode Current, I_k	75 mA
Beam Perveance	.0271 μperv
Frequency Range	59 to 64 GHz
Cold Bandwidth, B_c	34.3%
Cavity Period, L_c	0.0968 cm. (0.0381 in.)
Beam Hole Diameter, 2a	0.0559 cm. (0.022 in.)
Beam Filling Factor, r_o/a	0.35
At center Frequency:	
Phase Shift/ Cavity, BL_c	1.5 π radian
Pierce Impedance, K	7.094 ohms
Radial Parameter, α	1.312
Loss/ Cavity, L_{cav}	0.036 dB

3.1.2 RF Circuit Cavity Design

The two significant requirements driving the 961H and 961HA circuit designs were the need for high efficiency and wide bandwidth. With high efficiency a primary objective, a conventional cylindrical cavity configuration with reentrant ferrules was the preferred choice because of its high interaction impedance. The beam is focused through a center hole, whereas the RF wave travels along a serpentine path through coupling holes that rotate 180 degrees from cavity to cavity. This slows down the effective phase velocity of the wave to approximately that of the beam, allowing the transfer of energy from the electron beam to the RF wave. The axial electric field varies as exp ($i(\omega t-\beta z)$), where ω is radian frequency and β is the wave number. Omega (ω) and beta (β) are related via the RF cavity dispersion; the phase velocity of the wave is given by the ratio of ω to β. Amplification occurs in the region where the wave is synchronous with the slow space charge wave of the beam (which is slightly less than the dc electron speed). The extent that the wave and beam speeds differ and still achieve amplification determine the TWT bandwidth.

The coupled cavities effectively create an RF bandpass filter. A schematic of the RF cavity is shown in Figure 2. The upper cutoff frequency is at the single-cavity resonance and is determined primarily by the cavity inner diameter and the gap capacitance. The width of the passband is determined by the amount of coupling, which varies with the area of the coupling hole. As the coupling hole angle increases, so does the bandwidth, shifting the lower cutoff frequency downward. Increasing the ferrule gap moves the frequency band up with only slight changes in bandwidth. The beam hole radius has a major effect on the gain. The smaller the beam hole the more effectively the RF electric fields fringe into the beam interior and interact with the electron beam, which raises the gain. As the coupling angle and the bandwidth increase, the gain per cavity decreases.

A second special requirement for the tube was wide band performance. The ultimate objective was operation over the frequency range from 59 to 64 GHz. This requirement of 5.0 GHz bandwidth with high efficiency was challenging for a V-band TWT. As the passband is increased to achieve broad band performance, the phase velocity at the upper cutoff (the cavity resonance frequency) approaches the electron velocity, until at some point the tube becomes unstable. To ensure an adequate margin of stability, an initial cold bandwidth of approximately 35 percent was selected on the basis of prior experience with other millimeter-wave TWTs.

961H RF Circuit

To minimize risk on the 961H initial development, the first tubes were optimized for 2.5 GHz bandwidth (61.5 to 64 GHz); it was planned that two tubes could be used to cover the bandwidth. The center design frequency, 62.75 GHz, was placed at a phase shift per cavity of 1.45π radians. This value is somewhat higher than typically used in high efficiency TWTs, but it has the advantage of less phase velocity dispersion for improved bandwidth performance.

The two 961H TWTs (the baseline for the 961HA) both oscillated when operated at a cathode voltage near the design value of −19.7 kV. However, the TWTs were stable at some voltages lower and higher than the design voltage. The reason for both the instability and an anomaly at 65 GHz was that the upper cutoff of the slot mode, a high impedance point, lay almost exactly (and accidentally) on the voltage line passing through the design point. Hence, at the nominal design voltage of 19.7 kV, the tube oscillated at the upper cutoff of the slot mode (130 GHz). The design point is defined as the phase shift per cavity at center frequency. The frequency versus phase (ω-β) curve and line of constant phase velocity ("voltage line") are plotted in Figure 3. The design point is indicated by a cross. As the voltage was changed away from this value in either direction, the voltage line moved away from the high impedance point until the oscillation could not sustain itself.

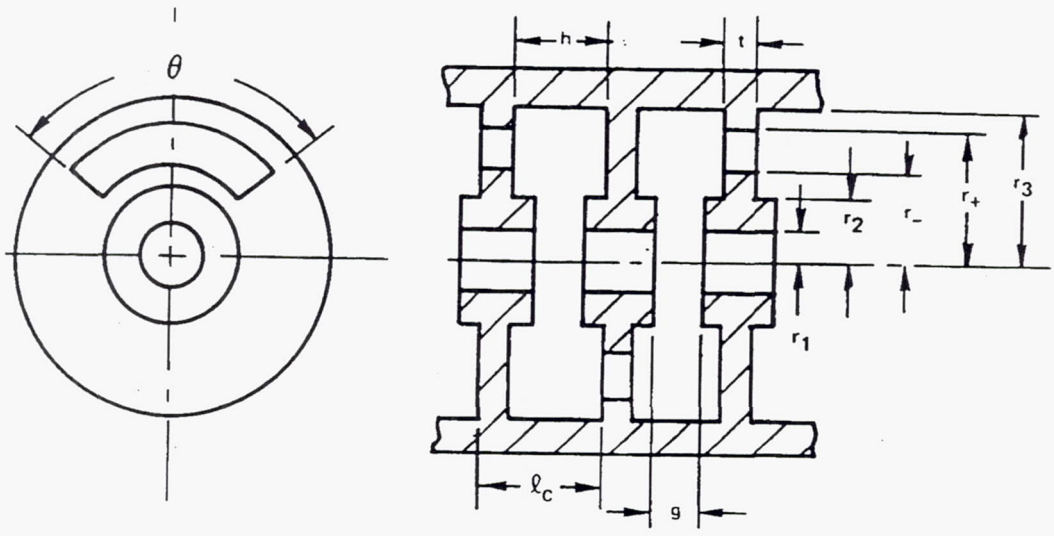

$2r_1$ – beamhole

$2r_2$ – ferrule diameter

$2r_3$ – cavity diameter

r_- – slot inner radius

r_+ – slot outer radius

θ – coupling angle

ℓ_c – circuit period

h – cavity height

t – web thickness

g – ferrule gap

Figure 2. 961HA RF schematic.

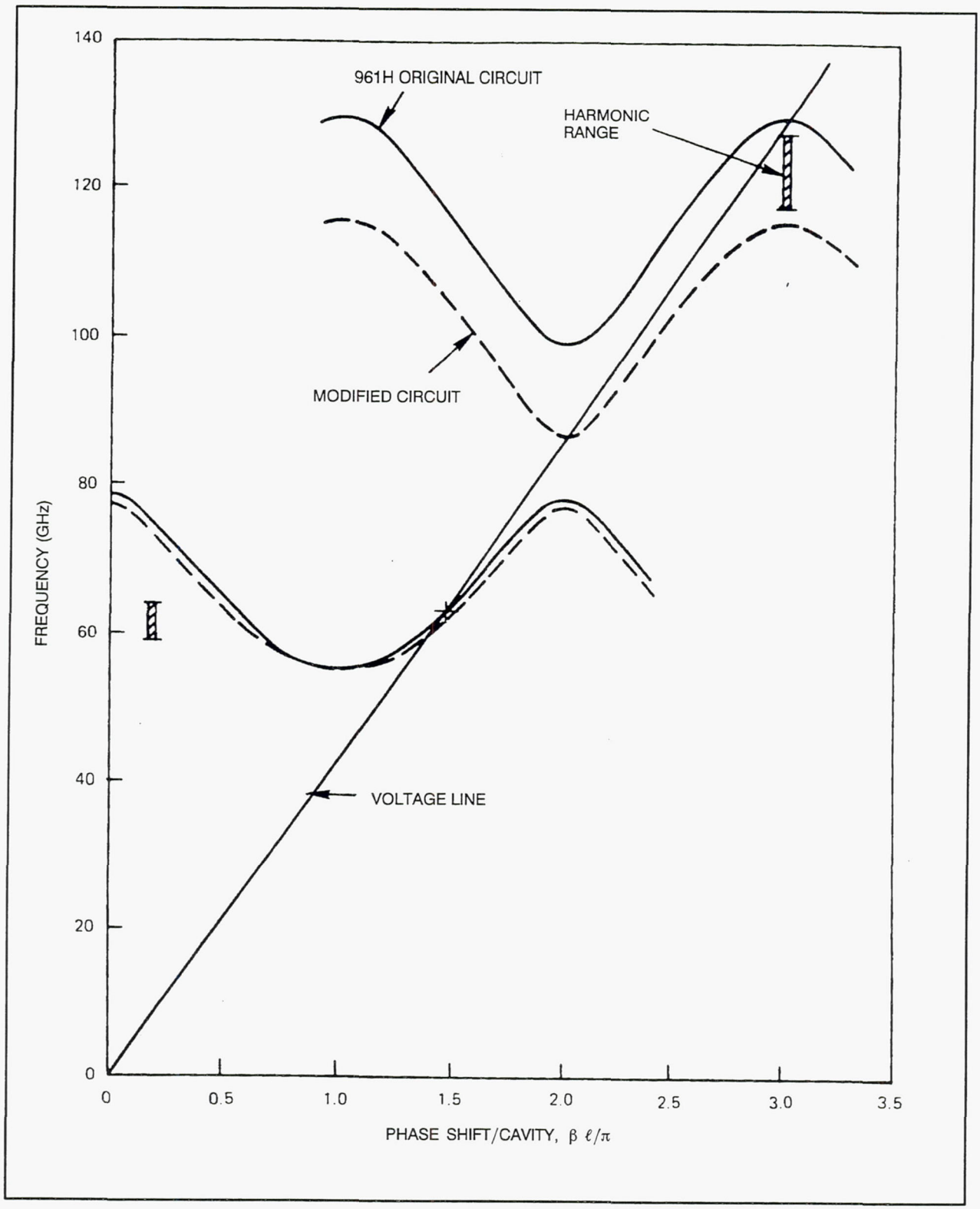

Figure 3. 961H passband characteristic.

Both 961H tubes also exhibited an anomalous power hole at about 65 GHz. The second harmonic of 65 GHz is 130 GHz, the upper cutoff of the slot mode. The mechanism for the power hole at large signal is the excitation on the electron beam of a second harmonic current component because of nonlinear effect at large-signal levels. (At low RF drive, the gain curve showed no clear-cut anomalous behavior.) If an upper passband provides amplification of the harmonic signal component, the beam modulation is changed, disturbing the growth of the signal at the fundamental frequency.

961HA RF Circuit

The cure for both 961H circuit problems was to shift the slot mode down in frequency, such that the entire harmonic frequency range is above the upper cutoff. This goal was achieved by increasing the inner radius of the coupling hole. This has the effect of lowering the slot mode upper cutoff frequency away from synchronism with the beam, which was the cause of the oscillation. Further, the second harmonic frequencies of the hot band are no longer in the slot band, eliminating a power hole caused by harmonic coupling. The center frequency was shifted from 62.75 GHz to 61.5 GHz to cover the entire 59 to 64 GHz operating band. The phase shift per cavity at the center frequency was increased from 1.45π to 1.50π radians to increase the hot bandwidth. These changes caused a slight decrease in interaction impedance and thus gain, necessitating a slight increase in the number of cavities. We also changed the velocity taper cavity distribution to optimize the power for the new cavity dimensions and phase shift per cavity.

Figure 4a shows the dispersion relations, the $\omega-\beta$ curve, of the standard and velocity taper cavities. In this figure velocity is proportional to ω/β. The purpose of the velocity taper cavities is to regain synchronism of the slow wave structure with the beam after the beam has slowed from giving up kinetic energy to RF power. Figure 4b shows the dispersion relation of the slot mode of the standard cavity. To prevent slot mode oscillations, the voltage line of the beam is above the upper cutoff of the slot mode. The second harmonics of the hot band are higher in frequency than the slot mode to prevent a power hole caused by harmonic amplification.

However, the 961HA S/N 3 exhibited a drive induced oscillation (DIO) at the high end of the band when overdriven. We have found on hot test that if the beam current is reduced the DIO can be eliminated. To recover the output power, we recommend that the monel in the output waveguide be replaced with copper, which would result in an increase in rf output power by a factor of 1.21 at 64 GHz (the worst case power point), and even larger factors at other frequencies.

3.1.3 Small Signal Gain Analysis

Using the cavity geometry, $\omega-\beta$ dispersion characteristic and interaction impedance as input data, the small-signal computer program was used to determine the number of cavities, hot bandwidth, and small-signal gain. The nominal power output of the 961HA was required to be 75 watts. Though only 35 dB of gain was required the design gain was higher to allow the TWT to be driven with commercially available drive power, about 0 dBm. Allowances were also made for saturation effects, launching losses, and the loss in gain due to severs.

The small signal computer code calculates the loss per cavity, the gain per cavity, and the small signal gain of each RF section. The small signal code model assumes an electron beam of uniform cross section. The ratio of the radius of the beam to the radius of beam hole, b/a, is an important assumption, the accuracy of which directly affects the program's results. By iteratively varying the number of cavities in each section, the desired small-signal gain characteristics, shown in Figure 5, were obtained. A nominal gain per standard cavity of 0.5 dB was calculated by the small signal gain code.

The cavity distribution was chosen to maximize the RF output power at the band edges, while not having excessive small signal gain in the output section (to minimize gain ripple and maximize stability). There

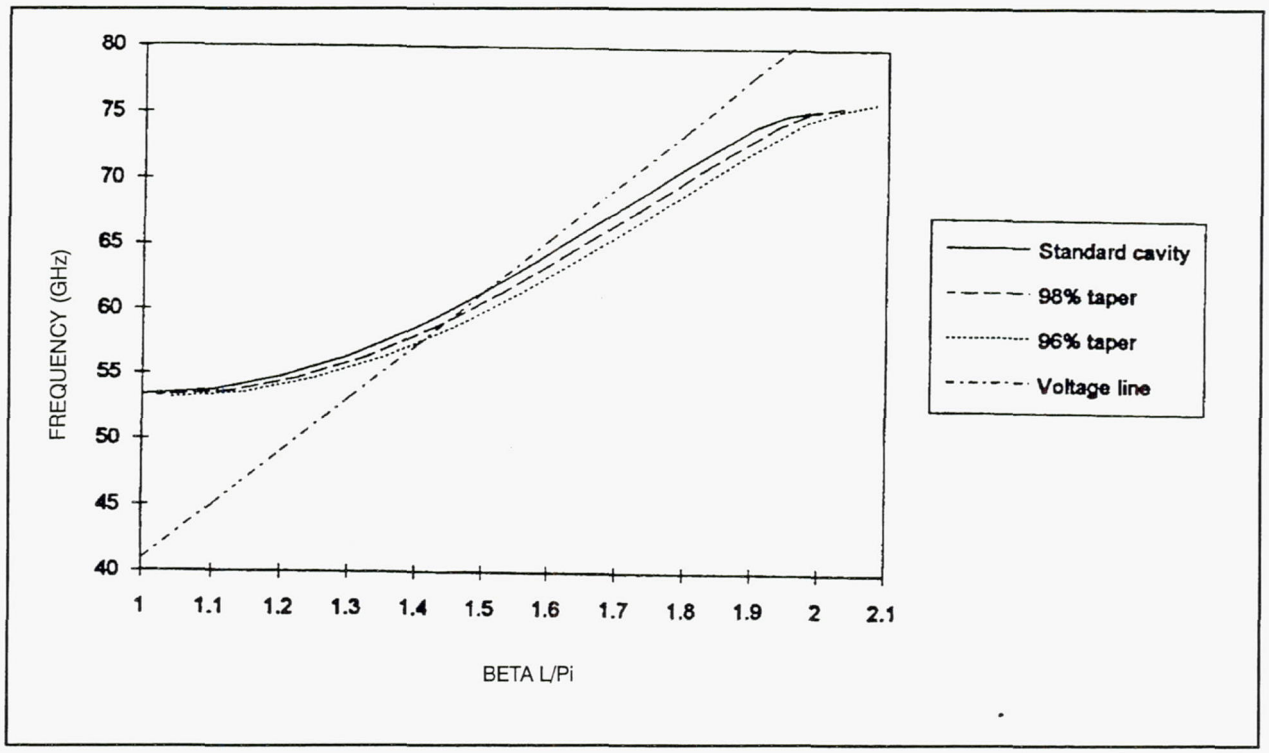

Figure 4a. The dispersion relations (ω-β) of the standard cavity, the 98% velocity taper, and the 96% velocity taper. Here L is the standard cavity Lc. The voltage line passes through the $\beta L/\pi = 1.5$ point of the standard cavity.

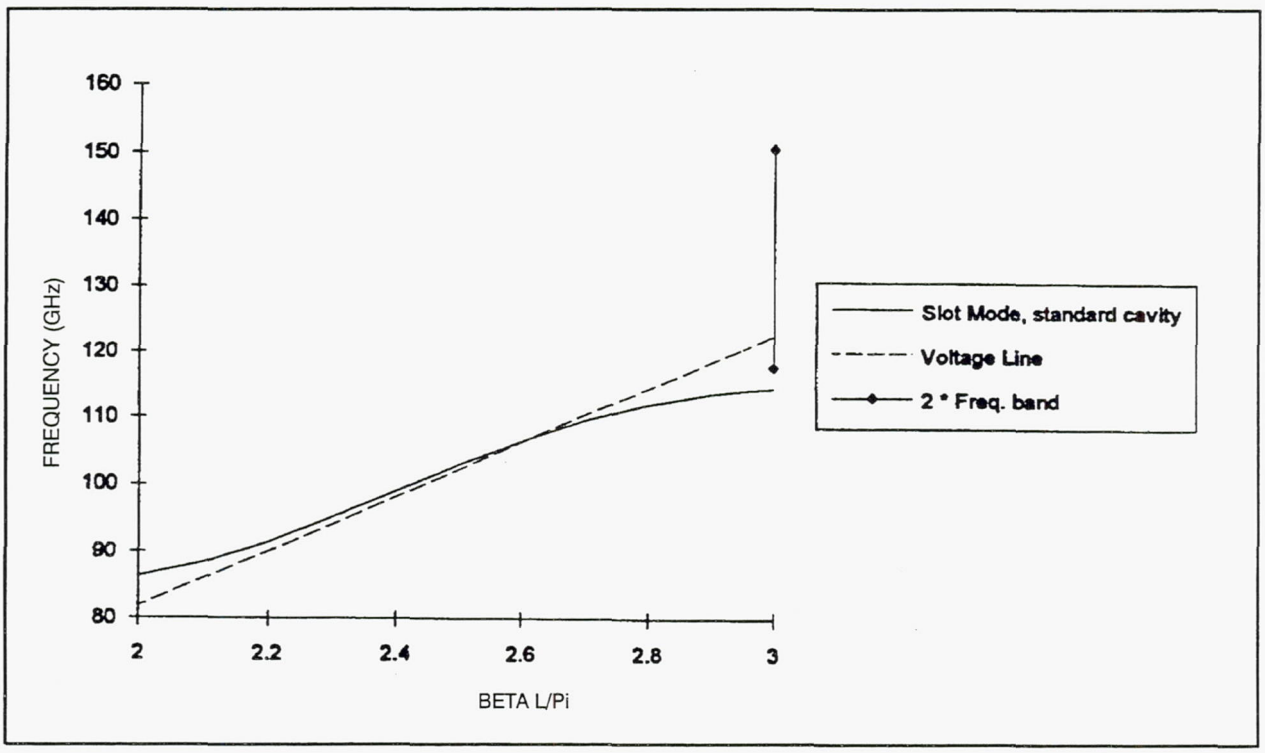

Figure 4b. The dispersion relation of the slot mode of the standard cavity. Both the voltage line and second harmonic of the frequency band are above the upper cutoff of the slot mode.

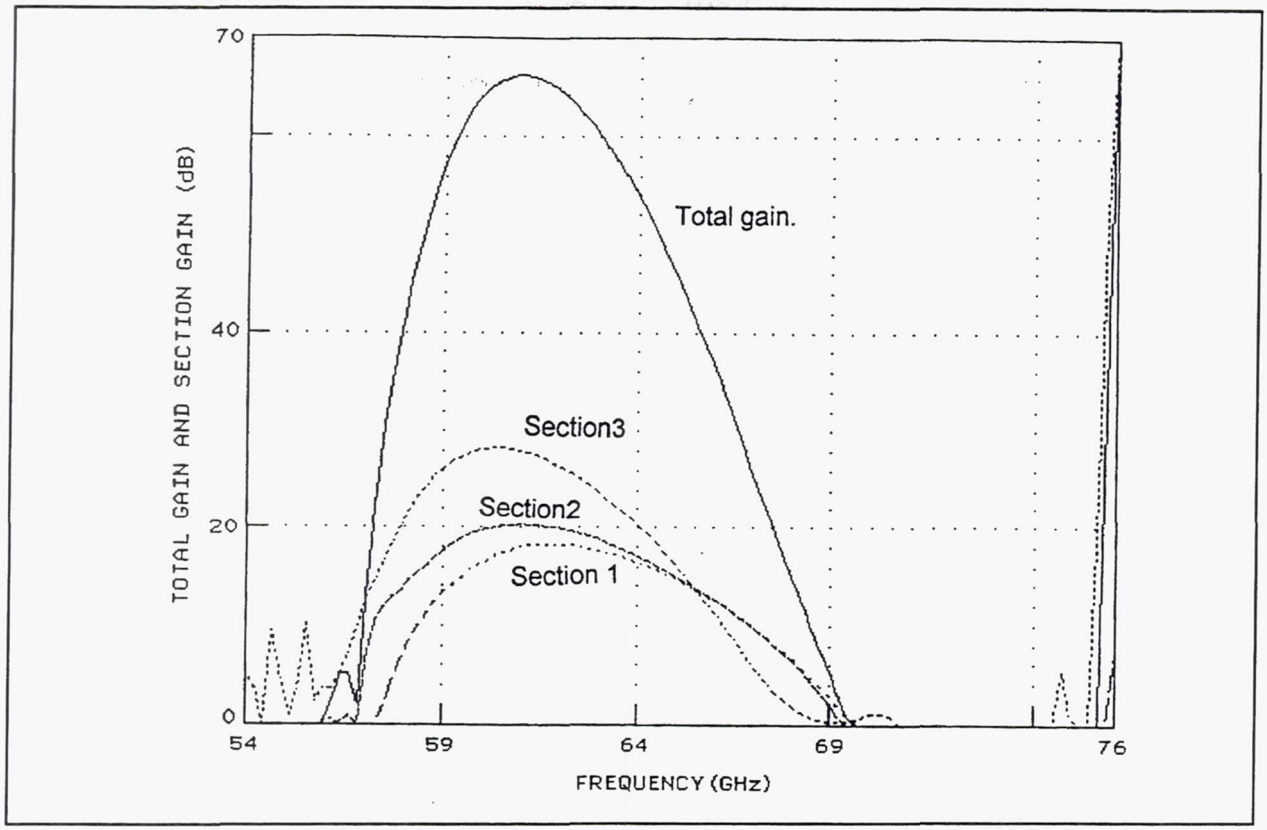

Figure 5. 961HA theoretical total small signal gain and net gain contributions of individual sections (b/a = 0.35).

is a trade-off between having sufficient gain beyond the sever of the output section at the upper band edge frequency to get good power, and minimizing the peak small signal gain. In the output section, the maximum small signal gain is 28.1 dB, and the small signal gain at 64 GHz is 20.4 dB. The input and center sections operate small signal, and there is no minimum requirement of gain beyond the sever. The peak gains of 18.2 dB and 20.4 dB in the input and center sections respectively cause little regenerative gain ripple.

The 961HA circuit has a total of 166 interaction gaps, or 160 RF cavities not including the terminations and match cavities. The 46 standard cavities chosen for the output section were to provide a balance between maximum efficiency and stability. An unequal number of cavities was chosen for the first and middle circuit sections, 49 and 47 respectively, to minimize gain variations. The final design cavity distribution (including the two velocity taper sections) for the 961HA TWT is shown in Figure 6.

3.1.4 Large Signal Analysis

The initial circuit configuration from the small-signal program was modeled by the large-signal program. The large-signal code predicts power output and efficiency. The cavity distribution, particularly the velocity taper, was further iterated until the output power versus input power curves at the band edges were nearly coincident. Two velocity tapers are included in the output section. As RF energy is extracted from the beam it begins to slow down. The velocity taper resynchronizes the RF wave to the slower beam. The 961HA has eleven 98% and eight 96% velocity taper cavities, including the output match cavity. The resulting large-signal output power versus RF drive power curves for the final circuit are shown in Figure 7 for mid-band and the band edges. These results were computed for a beam current of 75 mA and a

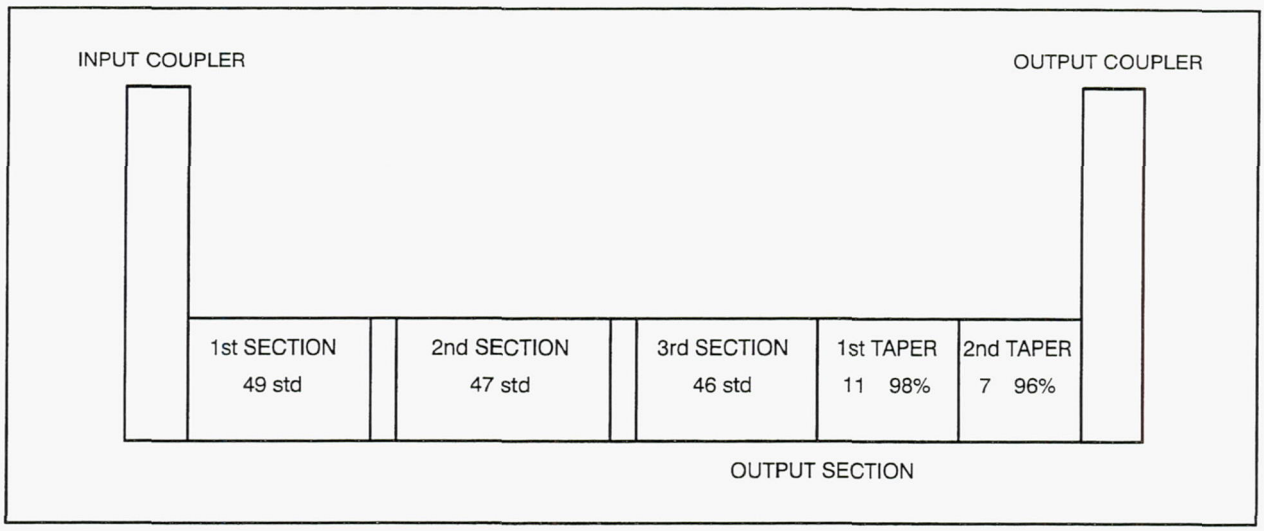

Figure 6. 961HA RF cavity distribution.

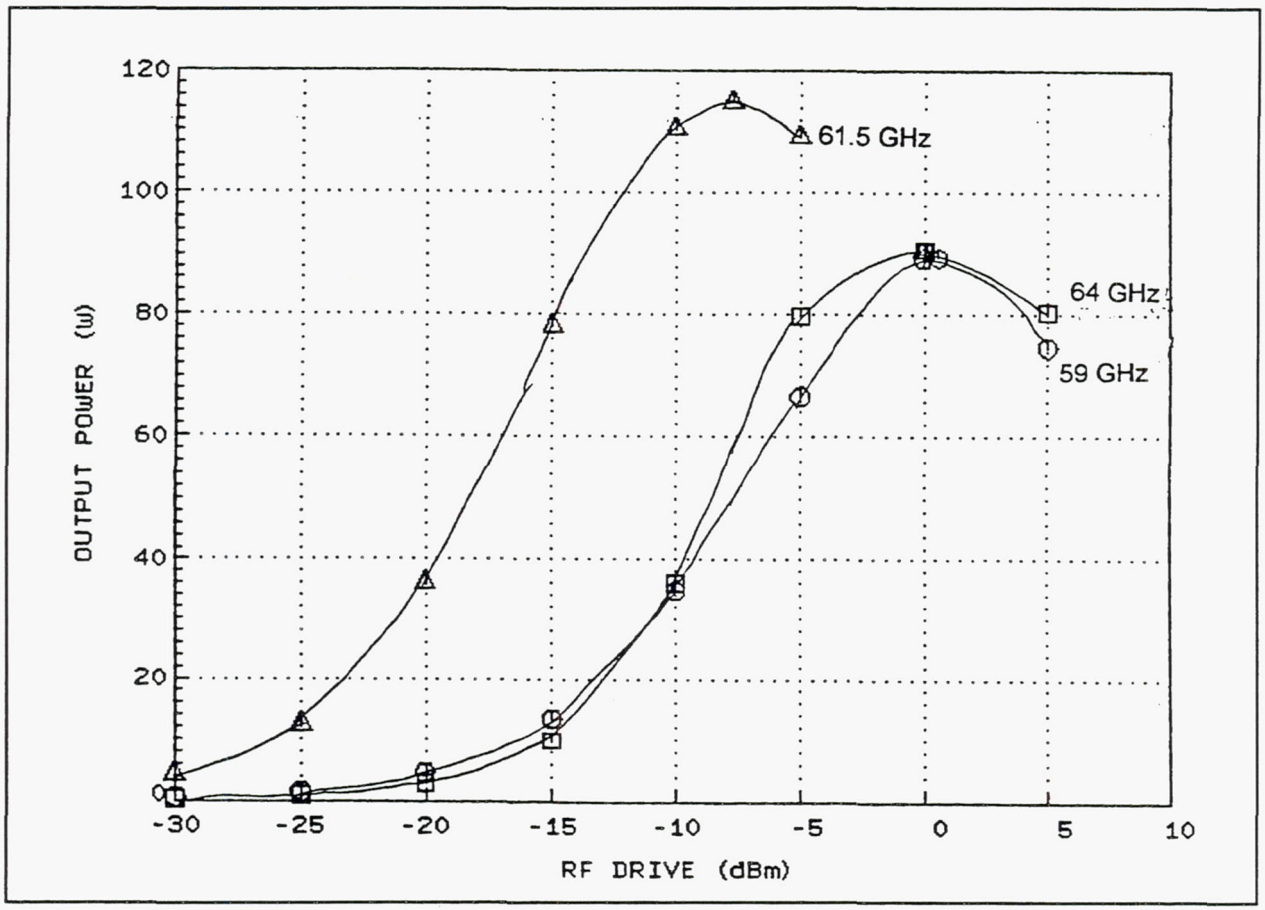

Figure 7. 961HA theoretical RF output power.

beam filling factor, b/a, of 0.35. From this plot we see that at constant RF input power, the 61.5 GHz center frequency is overdriven when the band edge frequencies are just saturated. A slight preference has been given in the design power to the 64 GHz upper band edge frequency over that of the 59 GHz lower band edge frequency, because the lower band edge power can be increased if necessary by increasing the cathode voltage, whereas changing the cathode voltage typically does little to change the upper band edge power.

3.2 ELECTRON GUN DESIGN

Over the course of the development of this V-band TWT there were three gun designs: the 262BMA single anode gun used on the two early TWTs, 961H S/N 1 and S/N 2, the 309BMA dual anode gun tested on the advanced TWTs, 961HA S/N 1 and S/N 2, and the 324BMA single anode gun tested on the 961HA S/N 3. The advanced design, the 961HA, unlike the 961H, required a low output power mode to be achieved by changing the anode voltage. A second anode is needed to maintain a continuous ion trap. The dual anode gun did not focus well, we believe due to magnetic end effects. Rather than revert to the original single anode gun, which had focused well but had inconsistent perveance, a more up to date single anode gun was designed for the 961HA S/N 3. This third gun focused well and achieved the design perveance.

3.2.1 The 262BMA Single Anode Electron Gun (961H)

The predecessor TWT, the 961H, had a single anode gun designated the 262BMA; the details are reported in ref. 1. The 961H was designed for the same cathode voltage as the 961HA tubes, but had only 70 mA cathode current. Two 961H tubes were built and tested. Both 961H tubes eventually focused well with 2.0 mA DC body current, and 3.0 to 3.7 mA of RF body current. However, S/N 2 had to be regunned once, and both S/N 2 guns were low in perveance.

3.2.2 309BMA Two Anode Electron Gun (961HA S/N's 1 and 2)

Initially a two anode gun, called the 309BMA, was designed to allow dual mode operation on the 961HA TWT. This gun incorporated newer construction techniques for better positioning of the cathode. Two dual anode guns were built and tested on the 961HA TWTs S/N 1 and 2. With the first anode grounded, in the high power mode, the cathode current was 70 mA. For the low power mode, the first anode was biased at -5 kV with respect of the tube body, reducing the cathode current to 49 mA. The second anode was biased 100 V positive with respect to the tube body; this slight barrier creates an ion trap to reduce cathode poisoning and erosion of the cathode M-coating.

The 309BMA and later guns were designed with the computer program THERMGUN. The earlier 262BMA gun was designed with a thermal program written by Kurt Amboss of EDD based on paraxial ray assumptions. THERMGUN is a finite element code based on Richard True's doctoral thesis at the University of Connecticut. Thermal electrons were added by Charles Thorington at EDD. Thermals are an important part of low perveance electron beams. This program has been used successfully to design many guns at Hughes.

In practice, the 961HA S/N 1 with the dual anode gun focused poorly, with 90% DC transmission, and 89% RF transmission, and even that was hard to achieve, requiring days of focusing. S/N 2 was even worse. In the latter tube, asymmetries were found, which may have been present to a lesser extent in S/N 1. The additional anode required that the first magnet be placed too far from the cathode. This required a too strong first magnet, creating magnetic field variations and a scalloping beam.

The original computer design model assumed that the magnet stack had no significant peak-to-peak variation in field. Further analysis including peak-to-peak field variations was performed. The

electrostatic beam minimum R_{95}, the radius enclosing 95% of all electrons, was 0.0017 cm. (0.0067 in.). The "throw", the distance from the cathode to the electrostatic beam minimum, was 2.197 cm. (0.865 in.). These numbers are not much different from those of the new single anode gun that focused well. However, the first magnet gap center was placed 2.423 cm. (0.954 in.) from the cathode valley, much farther than the 1.852 cm. (0.729 in.) of the new gun. The beam could not be made to focus on the computer without substantial ripple, and required a strong first lens to keep the beam from diverging, achieved by making the first magnet both strong and thick. The first magnet was 2400 Gpeak, and the rest of the magnets 3500 Gpeak. Because of the strong thick first magnet, this stack would have had a strong reversed cathode field were it not shielded by the iron first anode. It also had end effects (weak odd numbered magnets, strong even ones).

3.2.3 324BMA Single Anode Electron Gun (961HA S/N 3)

Because of the focusing difficulty of the first two 961HA TWTs and the fact that a dual mode requirement was no longer needed, it was decided to re-design the gun for optimum focusing with only one anode. Rather than revert to the original 961H single anode gun, the 262BMA, a new gun, the 324BMA, was designed that would incorporate the mechanical improvements of the dual anode 309BMA gun. The two anode 309BMA gun had a slightly larger cathode, for less cathode loading and longer life. It also had a step in the focus electrode next to the cathode, allowing the amount of cathode recess into the focus electrode to be more accurately measured. This is an important parameter. Excessive cathode recess was a possible reason that the original single-anode 262BMA gun on 961H S/N 2 of the previous contract was 15% low in perveance. In contrast the dual anode 309BMA gun (used on 961HA S/N 1) had the correct perveance (cathode current = 70 mA). This also allowed many of the same parts to be used.

Removing one anode allowed the first magnetic gap center to be more optimally positioned closer to the cathode. Further, this was achieved with a weak standard thickness first magnet, which minimized the cathode magnetic field and also end effects. The magnets were ordered individually, rather than as a stack, so they were interchangeable. The anode was moved closer to the cathode to increase the cathode current from 70 to 76 mA (to compensate for a lossier output coupler). The 324BMA design parameters are listed in Table 3.

TABLE 3. 324BMA ELECTRON GUN DESIGN PARAMETERS

Cathode voltage	-19.7 kV
Single anode (ion trap) voltage	+ 100 V
Cathode current	76 mA
Cathode loading	2 A/cm^2
Beamhole ID (2a)	.0558 cm. (0.022 in.)
Electrostatic $r_{95\ min}$	0.01618 cm. (0.007362 in.)
Cathode to electrostatic r_{95min}	2.107 cm. (0.8294 in.)
Cathode valley to the center of the first magnetic peak	1.852 cm. (0.729 in.)
Peak magnetic field	3560 G (except first magnet is 1580 G)
Magnetic period (L_m)	0.965 cm. (0.380 in.)
λ_{sc}/L_m	1.41
$r_{99.5\ max.}/a$	0.64

On hot test the 324BMA gun on the 961HA S/N 3 TWT focused well and easily. With the collector depressed, the body current is only 2.0 mA DC, 3.0 mA RF , out of cathode current of 76 mA. The cathode current was eventually decreased to 74 mA by operating the heater power closer to the knee, for RF performance reasons explained in Section 4.3. The body current is the same at 74 mA.

In the 961HA TWT the beam hole begins before the beam has fully converged. Figure 8a shows that the beam grazes the beam hole at the entrance, with some interception there likely (the tube feels warm at the input). There is a compromise between the beam amply clearing the beam hole at the entrance and in minimizing the ripple downstream. This design emphasized minimizing the ripple. Focusing would be better if the input adjustable ferrule (Figure 9) could be moved farther from the cathode and/or opened up without moving the center of the first magnetic gap. The two anode gun did have the adjustable ferrule placed farther away and its beam did not graze it, but since the first magnet was too far away, the beam rippled and focusing was poor.

The cathode loading of the 262BMA gun was probably non-uniform, with a high cathode loading at the cathode outer diameter. This is because the cathode in the 262BMA was only recessed 0.00102 cm. (0.0004 in.) into the focus electrode. The 324BMA gun is recessed more, 0.00660 cm. (0.00260 in.), producing the fairly uniform cathode loading vs. radius shown in Figure 10. The 324BMA gun is less sensitive to variations in the amount of recess, because the current density is less at the cathode outer diameter.

3.2.4 Electron Gun Mechanical Design

The mechanical layout of the 324BMA electron gun is shown in Figure 11. The vacuum envelope of the gun is made of high-purity aluminum oxide ceramic cylinders brazed to Kovar rings. The ceramics are grooved on both the inside and outside surfaces to increase the electrical standoff and to provide shadowing against line-of sight-barium emission, which might be deposited during the life of the tube. Kovar, an iron-nickel alloy, is used for the weld rings because it closely matches the thermal expansion of the ceramics and welds easily. The anode is made of iron and the anode support cylinder of kovar to magnetically shield the cathode.

The cathode support cylinder is made of a molybdenum-rhenium alloy. It is brazed, along with the heat shields, to the Kovar cathode hanger. The cathode vendor is responsible for maintaining the concentricity between the cathode and cathode hanger. This eliminates a welding operation and achieves better tolerance control. The focus electrode is welded to the cathode support assembly and then this entire inner gun assembly is welded into the gun stem. The final assembly step is to RF braze the anode in place.

3.2.5 Magnetic Focusing

The 961HA TWT employs a periodic permanent magnet (PPM) focusing configuration using high coercive force samarium cobalt ($SmCo_5$) magnets. The determination of the rms magnetic field strength, Bo, was based on Herrmann theory. Several different strength magnet stacks were available to alter the field lower or higher if needed for focusing. The later electron guns were optimized into the measured magnetic field of 3500 Gpeak.

Due to the focusing problems associated with the 961HA dual anode TWTs, the focusing structure design was modified for the 961HA S/N 3. The first entrance magnet, which was thicker than the standard cell, was thinned down considerably. Also this magnet was sized in such away that end effects, variations in the peak-to-peak magnetic field of odd and even magnets, were reduced or eliminated. The first magnet is 1580 Gpeak and the remainder of the stack 3560 Gpeak.

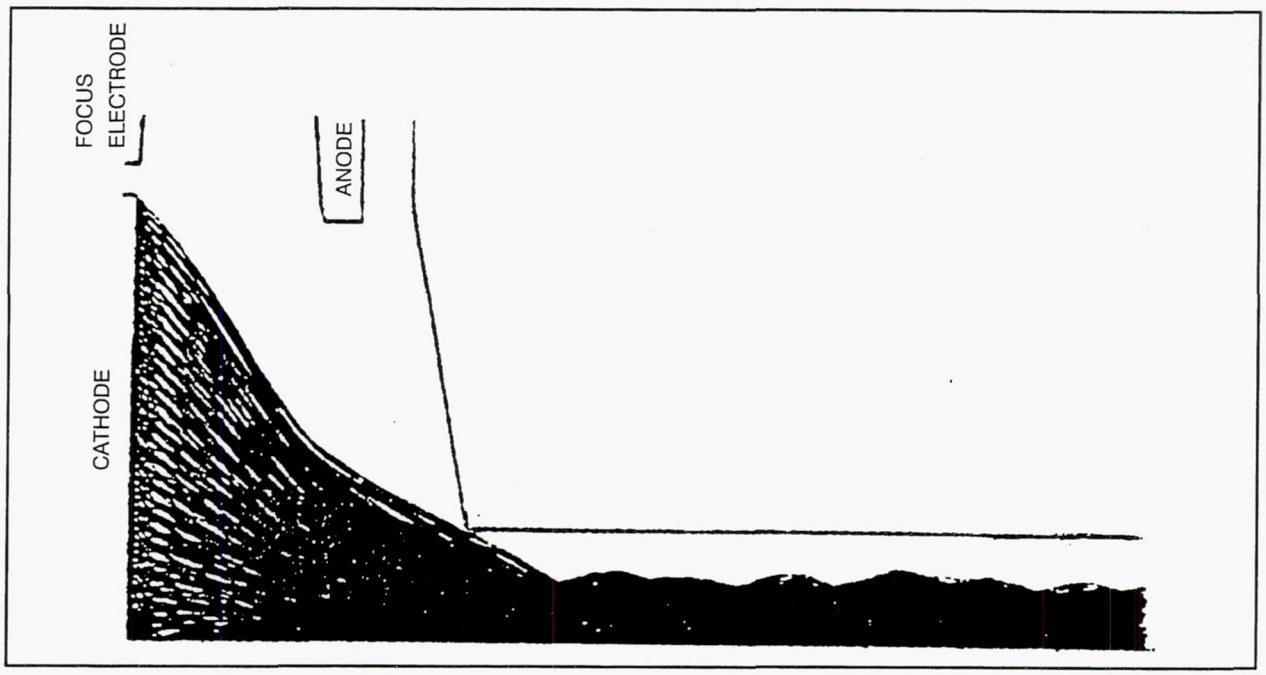

Figure 8a. 324BMA electron gun beam trajectories.

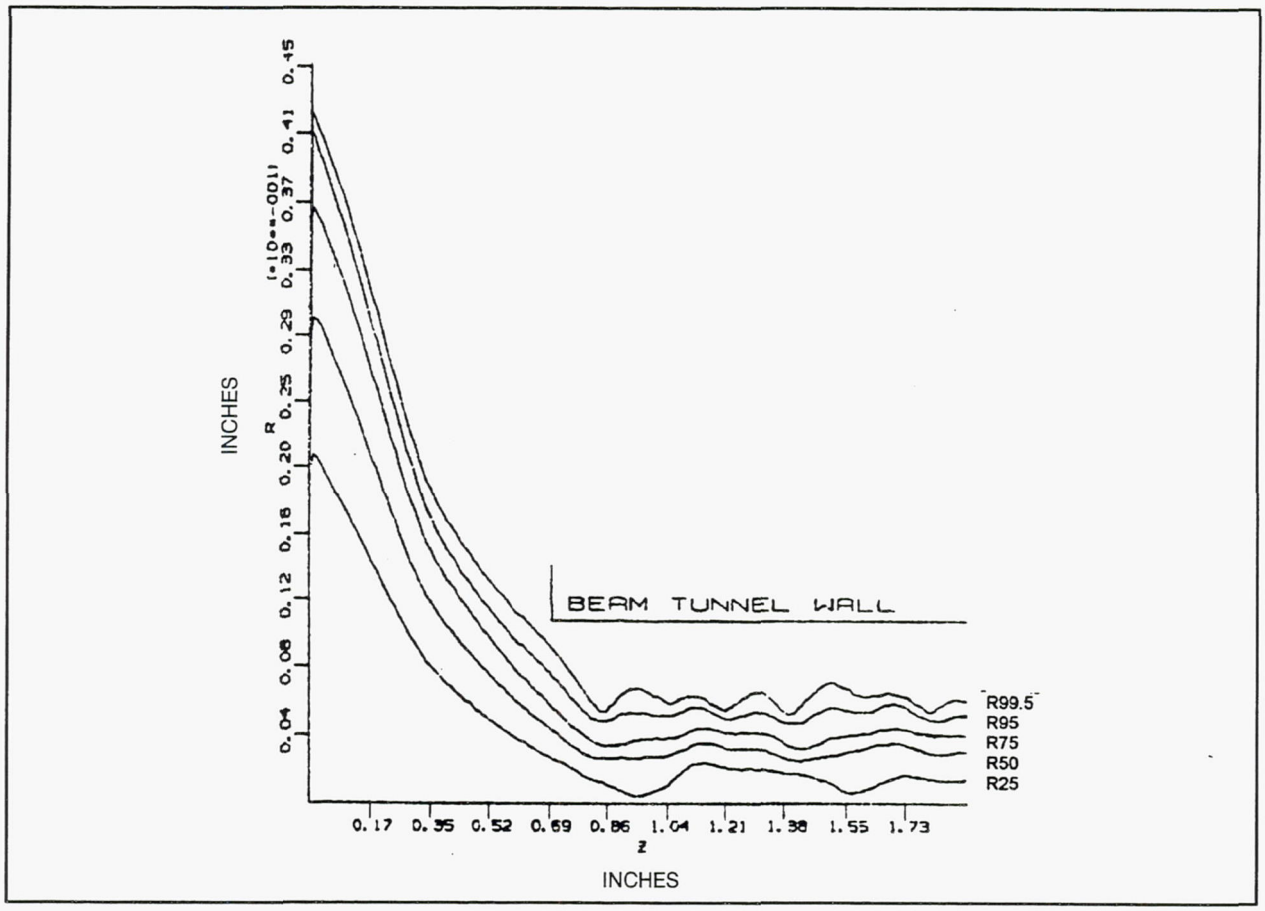

Figure 8b. 324 BMA electron gun statistical beam radii.

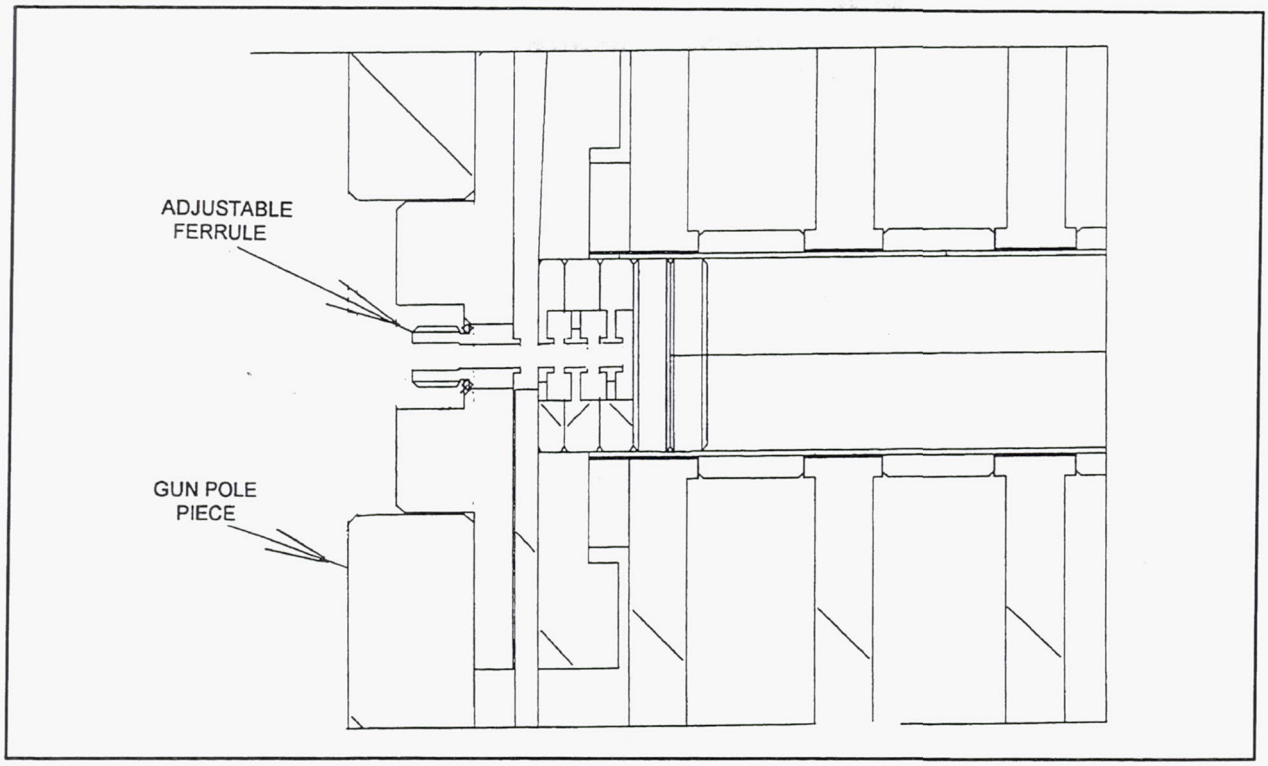

Figure 9. 961HA input coupler with adjustable ferrule.

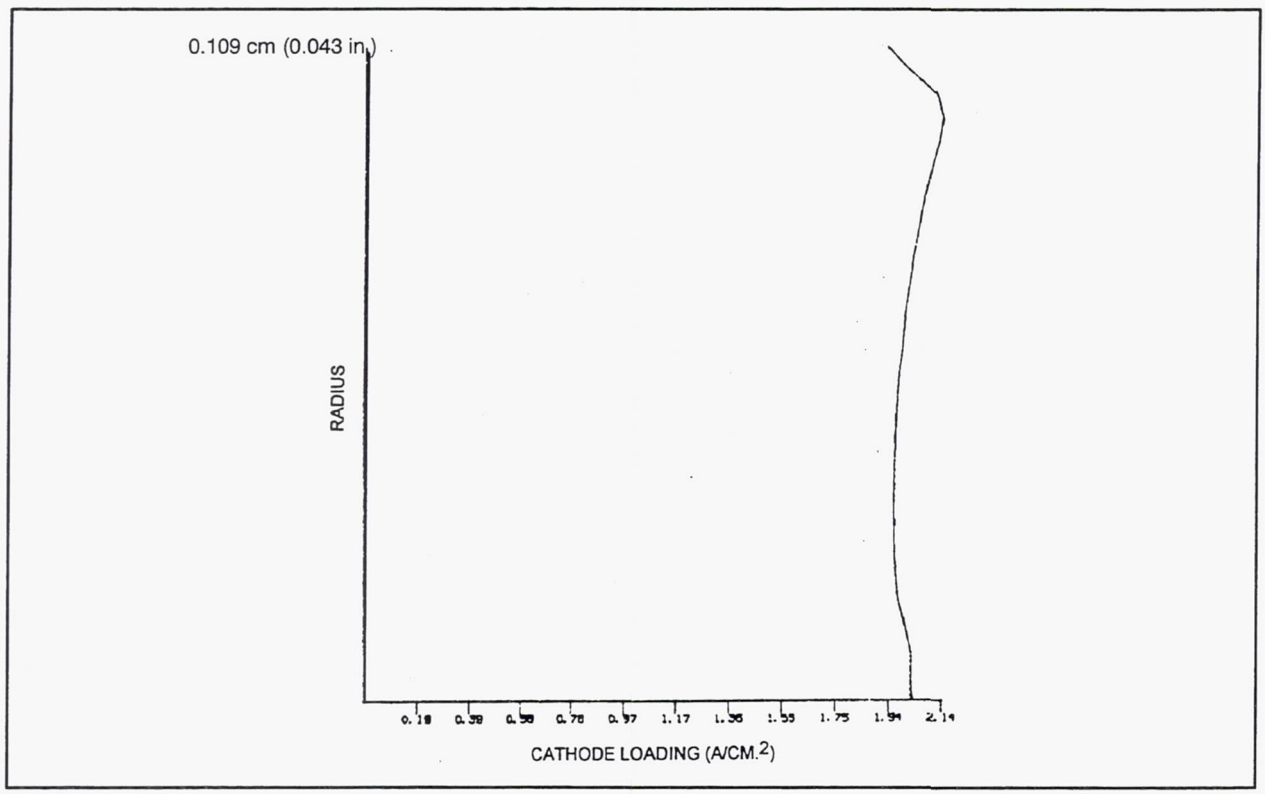

Figure 10. 324BMA electron gun cathode loading vs. radius.

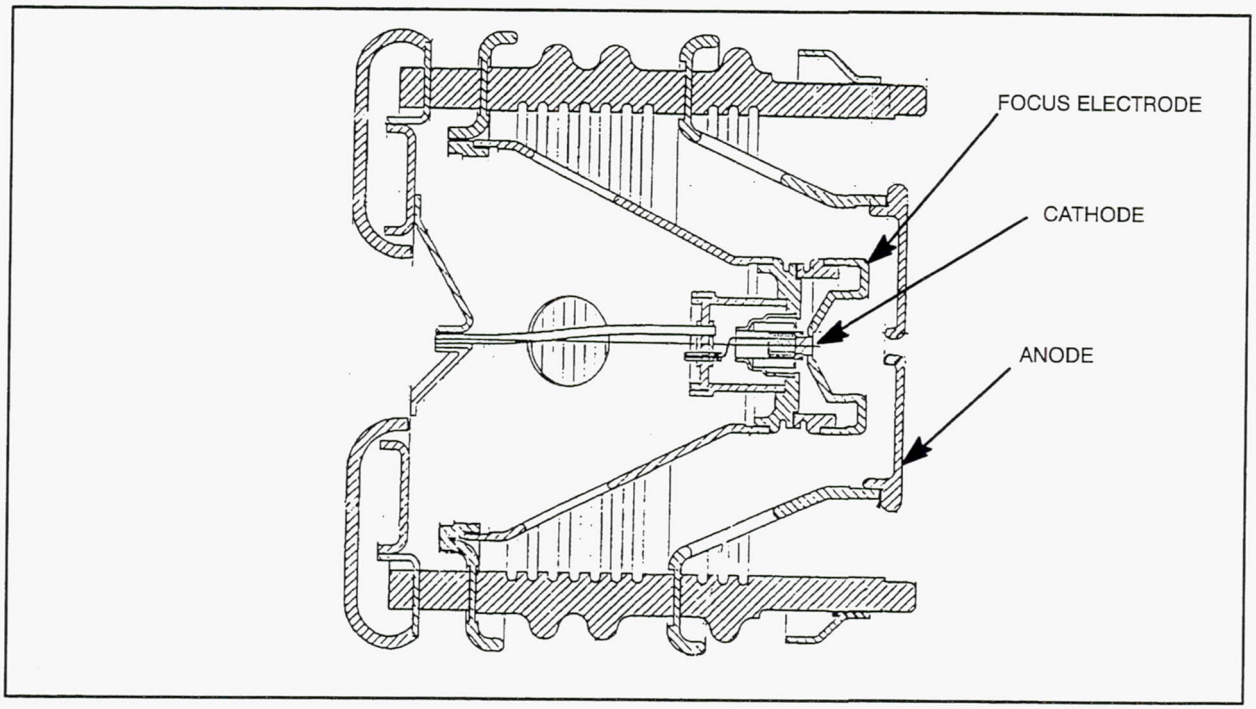

Figure 11. 324BMA electron gun mechanical layout.

The focusing structure, shown schematically in Figure 12 and in a photograph in Figure 13, is an integrally brazed assembly located external to the RF circuit. This structure also serves to provide vacuum and mechanical integrity for the TWT. The whole focusing structure consists of pole pieces, spacers, an inner liner, or sleeve, and heat risers for heat sinking to the baseplate. Vacuum melted electrolytic iron pole pieces are used to obtain the highest possible saturation flux density. The pole pieces are copper plated to avoid corrosion. The structure is honed to the final inner diameter for good alignment with the circuit.

Effective on 961HA S/N 3 the mechanical design was changed to build the focusing structure in two halves. We had great difficulty getting the 961HA S/N 1 and S/N 2 vacuum tight. The VSWR of both tubes degraded during multiple braze repairs. The need to simultaneously braze the input and output circuit to the focusing structure made for a difficult braze. Even with radiation shielding, the measured temperature variation along the length of the circuit was as high as 40 °C. One end is hotter and suffers excessive braze flow, while the cooler end may not flow well enough to seal. By splitting the focusing structure, the braze joint to both circuits can be better controlled. The final vacuum envelope is then formed by welding the center pole piece together.

3.3 MULTISTAGE DEPRESSED COLLECTOR

A high efficiency collector design was essential to reaching the goal of 40% overall efficiency since the RF efficiency of the TWT is less than 8%. Features of the collector design that contribute to the high efficiency are the relatively small velocity spread in the beam, a large collector-to-beam radius ratio, and the suppression of low energy secondary electrons by the use of isotropic graphite electrodes.

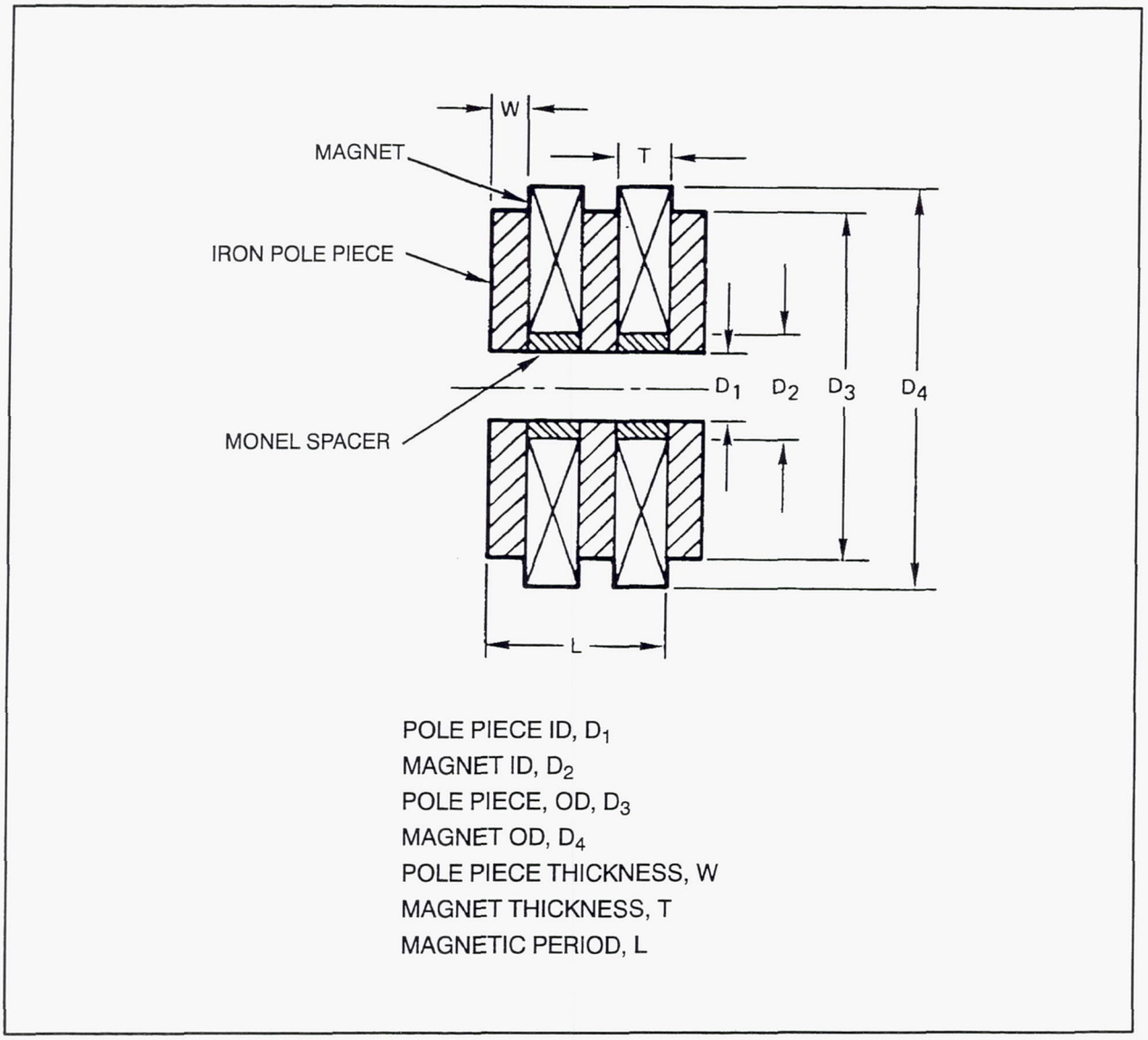

Figure 12. 961HA focusing structure schematic.

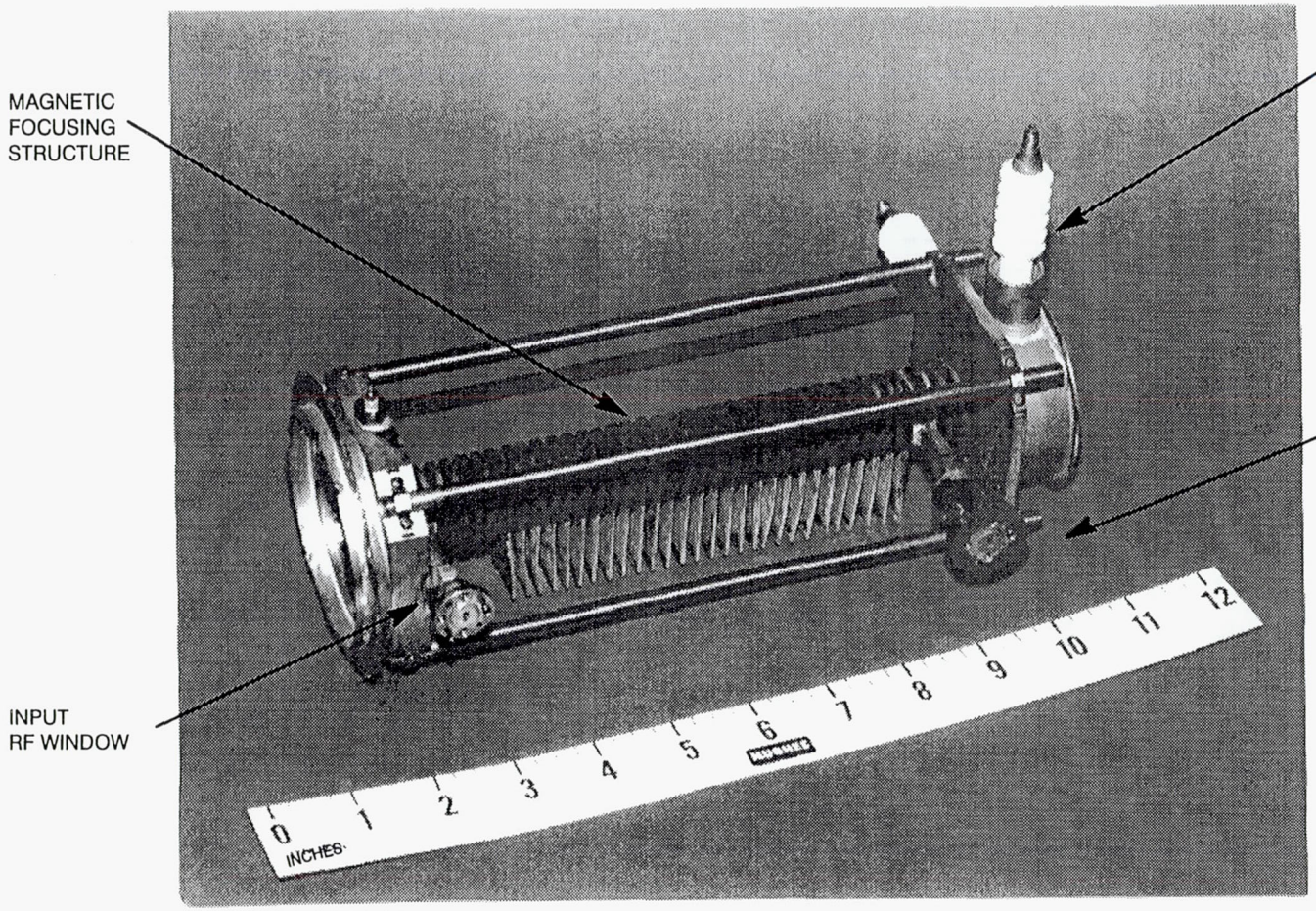

Figure 13. Photograph of 961HA focusing structure.

3.3.1 Collector Optics Design

The optics design of the 961HA collector was performed by NASA (see References 2 and 3). The NASA 2.5 dimensional large signal coupled-cavity computer model was used to calculate the interaction of the RF circuit field and magnetic focusing field with the electron beam. In the NASA model the beam was simulated by a series of 24 discs extending over an axial distance of an RF wavelength, with each disk divided up to four axially symmetric rings (the innermost ring is a disk). The RF circuit fields and electron ring trajectories are determined from the calculated axial and radial space-charge, RF, and PPM focusing forces as the rings pass through the sequence of cavities. The model was used to determine the trajectories of each of the rings at the RF output. This same procedure was then applied to the drift section between the end of the RF circuit and before the collector. The drift section is three magnetic half-periods long and larger in diameter than the RF cavity beam hole.

Finally the trajectories were calculated in the collector itself. The Herrmannsfeldt electron trajectory program was used. Each electron ring trajectory was treated as a continuous ray of current. The trajectory calculations were continued until the current rays impacted the electrodes. The effect of secondary-electron emission from electrode surfaces was analyzed by injecting reduced charges at the point of impact of the primary current rays and tracking their trajectories to their final termination within the collector. Based on the final location of all charges the recovered and dissipated power were calculated.

The collector was optimized for the high-power mode by primarily using the beam-RF interaction model results from saturated operation at midband. The final design trajectory plot in shown in Figure 14. These results were for the final (2nd) MDC design used with S/N 2 and 3. The computer design had the collector voltages at, -15.35 kV (E_{b1}), -16.8 kV (E_{b2}), -18.0 kV (E_{b3}) and the last stage a spike at cathode potential, (nominally -19.215 kV). The calculated collector efficiency (percentage of power recovered from the spent beam) is 94.7%. The same result was calculated for the low power mode. The calculated overall efficiency at 61.5 GHz was calculated to be 51% in the high mode, with zero beam interception. Allowing for 2% beam interception and assuming circuit losses of 20%, the model gave a value of 44.8% for the overall efficiency in the high power mode.

3.3.2 Collector Mechanical Design

The primary mechanical design concerns were the overall collector size because of weight and high voltage standoff. A traditional multistage collector design was employed consisting of a stepped alumina ceramic cylinder used to active metal braze the four graphite electrodes as shown in Figure 15. This design was suitable for collector construction with the two different configurations of graphite electrodes and provided ease of manufacture and accurate control over dimensions, spacings and alignments. The electrodes are made of POCO Graphite, grade DFP-2 isotropic graphite and are processed such that the impurity level is less than 5 ppm ash content. The material has an open and interconnecting porosity, which expedites outgassing during vacuum bakeout. Its coefficient of thermal expansion is such that direct brazing to an alumina ceramic was possible. Collector subassembly consisted of brazing the pre-machined and untextured graphite electrodes in a vacuum furnace using Ticusil as the braze alloy to the alumina ceramic, copper outer shell and the electrode leads. The collector assembly was completed by welding the high voltage feedthrus to the assembly.

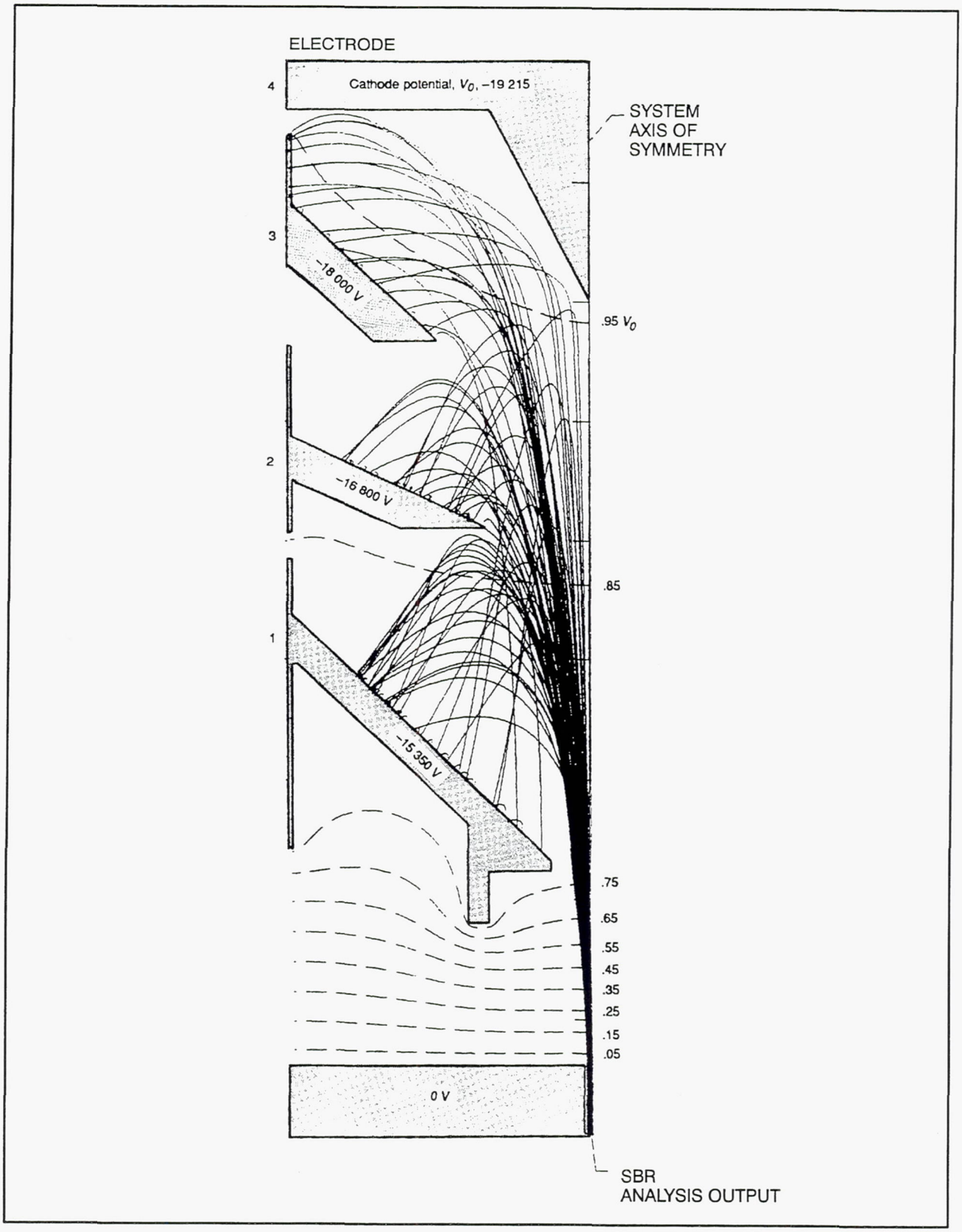

Figure 14. Charge trajectories in final four-stage 961HA collector design with TWT operating at saturation at mid-band (61.5 GHz).

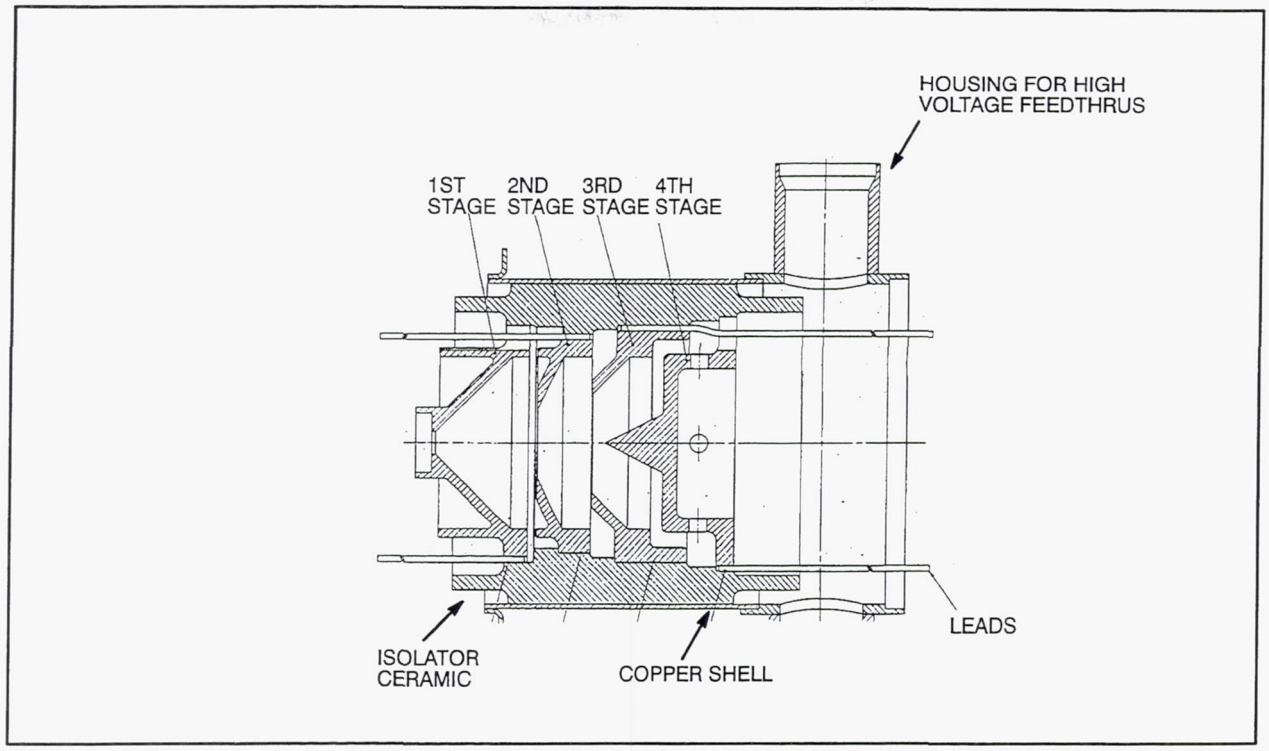

Figure 15. Collector Cross Section.

3.4 RF WINDOWS AND WAVEGUIDE TRANSITIONS

Two different types of RF windows and waveguide transitions were used on the 961HA. The first tube and the output section of S/N 2 were built using the 961H design. The 961H window consisted of a half-wavelength beryllia block window. Circular matching irises were incorporated to adjust the match of the window to the required frequency band. The waveguide transition was made of copper and had machined steps to transition to the impedance of the circuit. This waveguide and window design required many braze sequences to complete. The matching ferrule, though adjustable, was a press fit push/pull design that was difficult to position. The match would degrade at each assembly braze step. The probable cause was that deformation of the soft copper and buildup of braze material affected the critical matching dimensions.

The output circuit of the 961HA S/N 3 was built using a more modern V-band window and waveguide transition. The coupler transitions to the circuit impedance by tapering in width and height. The match coupling angle is a regular circuit part that locates into the coupler. This coupler can be leak checked as a subassembly. The earlier design was not a vacuum joint until after brazing to the circuit. The adjustable ferrule was threaded for easier positioning and an adjustable backwall was incorporated to optimize the VSWR. An iron adapter on the coupler allowed the RF window to be induction brazed to the tube, eliminating a furnace braze. The waveguide material is monel, a copper-nickel alloy. Monel is much stiffer than copper. The output window of S/N 3 is a cylindrical half wavelength alumina window. The circular design and the use of alumina ceramic results in higher yield because it is easier to obtain good fits and metallization.

However, other than the circular waveguide, which is copper, the rest of the window, the base and the mounting flange, are monel, as is the waveguide taper. The disadvantage of monel is that the RF losses are

higher than in copper. The beam current was increased on S/N 3 to compensate for this higher loss. However, at the higher beam current the tube had a drive-induced oscillation at the high end of the operating band. The beam current was reduced for stable constant input drive performance. The additional loss due to the monel coupler and window is estimated to be 0.9 to 1.05 dB depending on frequency. RF output power could be increased by corresponding amounts if a low loss waveguide could be designed to endure the rigors of the braze assembly process. We think that building the focusing section in two halves, as described in Section 3.2, may eliminate the need for monel waveguides. This is because the temperature difference between the input and output couplers during brazing is eliminated, since they are brazed separately, allowing better brazes and reducing the need for multiple re-brazes. Other millimeter-wave TWTs are now being built at Hughes to test this philosophy.

3.5 PACKAGE AND MECHANICAL DESIGN

The 961HA is packaged consistent with its space application. It is similar to the package concept used on Hughes most recent space TWTs at 60 and 94 GHz. (the 962H, 964H, 965H and 987H) This design configuration has passed space qualification for thermal/vacuum operation and vibration test as part of these other programs. No environmental tests were performed on the 961HA. What the 961HA package has in common with the other models are the following features:

1. The vacuum assembly is mounted in a baseplate that serves as a heat transfer medium between the tube and the mounting platform, and also serves a a structural backbone for the packaged TWT.
2. The RF circuit is cooled by means of copper heat risers brazed to the focusing structure and soldered into slots on the baseplate. This serves to effectively cool the circuit and provide rigidity without causing any thermal distortions of the circuit. Four support rods extend from the gun to the collector for additional rigidity prior to packaging.
3. The electron gun and multistage collector are clamped into a cradle, which is an integral part of the baseplate, for both support and heat transfer.
4. The electron gun is enclosed in a externally grounded vacuum can with "spark-plug" style high voltage feedthrus providing the electrical interface.
5. The collector has the same style high voltage feedthrus as the electron gun.
6. The internal high voltage insulation is provided either by ceramic member or vacuum spacing. No potting is used for voltage insulation purposes.
7. There are two ion pumps, one at the gun end and another at the collector end, for improved reliability.

The packaged 961HA S/N 3 was shown in Figure 1. The 961HA installation control drawing is shown in Figure 16.

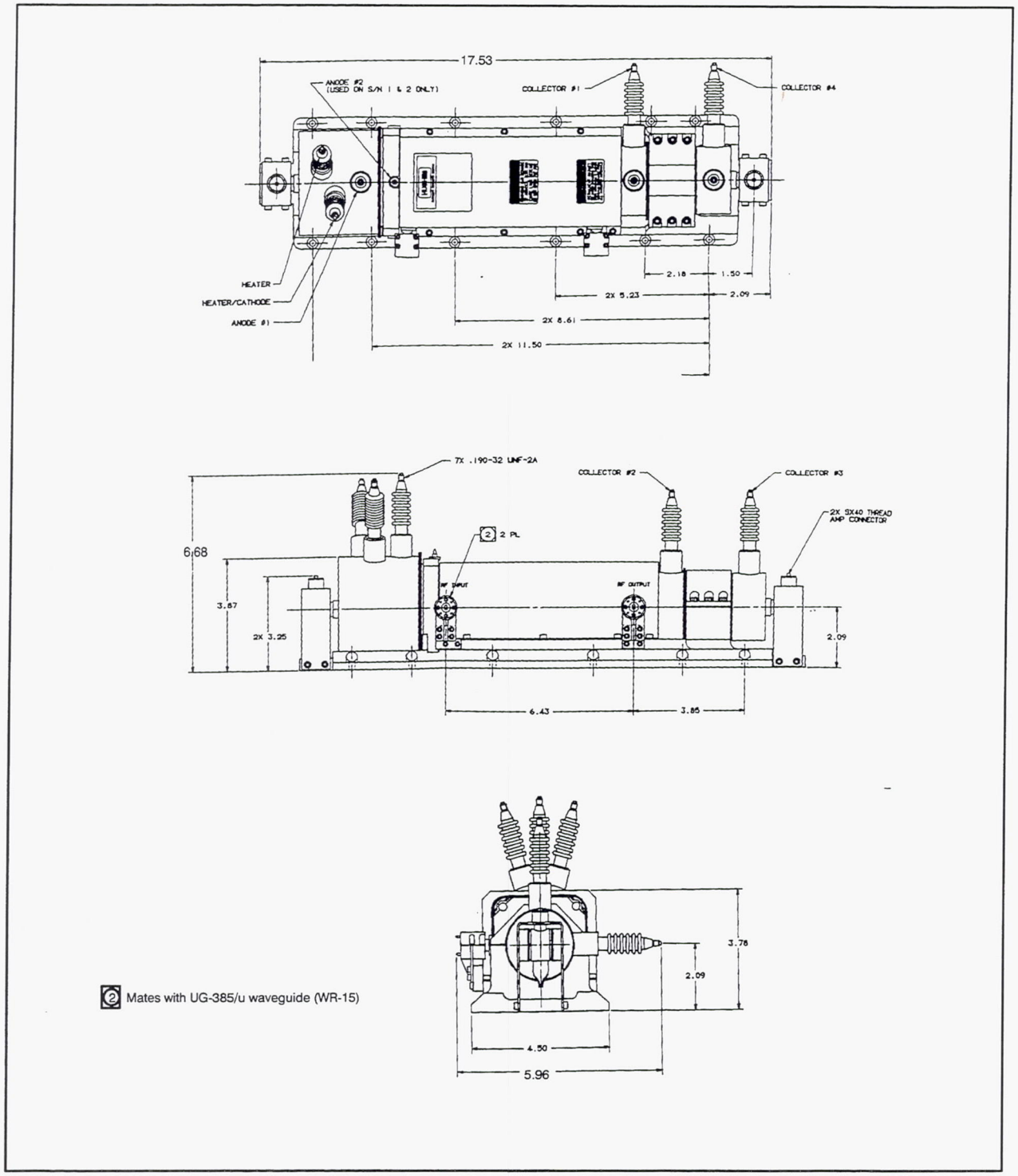

Figure 16. 961HA Installation Control Drawing.

4.0 TWT AND MDC TEST RESULTS

The changes made between the 961H design and the 961HA design were to implement the full 5 GHz bandwidth, to incorporate the refined collector design, and to implement dual power mode performance by incorporating a second anode. The first tube demonstrated that the bandwidth, output power, and efficiency goals were achievable. However, the focusing of S/N 1 was inadequate to process the tube CW. The focusing of the second tube was not as good as the first. After a failure analysis that looked at both the optics and mechanical alignment of the gun, many changes were made to improve the VSWR and focusing of the TWT. These changes were successful. S/N 3 focused well and achieved near goal output power across the band. A new coupler, used to provide a more rigid interface for VSWR quality, reduced the output power by adding resistive loss. Though the beam current was increased to reach the design value of output power, it was not enough. Also the higher beam current reduced the stability of the tube. At a beam current needed to achieve 75 watts across the 5 GHz bandwidth, 80 mA, and for a constant input drive power, the tube would have drive-induced oscillation at the higher frequencies. The tube was first aged with 74 mA beam current at a constant input drive of −3 dBm. Then the tube was aged to saturation, avoiding inducing oscillation at the higher frequencies. The tube was packaged and Acceptance Tested at 74 mA cathode current, demonstrating higher CW output power over a wider frequency band than previous space V-band TWTs.

4.1 961HA S/N 1

The construction of the 961HA S/N 1 was difficult. The mechanical design of the coupler required excessive braze runs even if everything went right. However the stack braze required multiple attempts to obtain a vacuum tight seal. When the tube was finally sealed the output VSWR had increased to 50%. Though this match was expected to result in unacceptable RF performance, the TWT was processed to test in order to obtain focusing data and to verify that the instability and harmonic interaction of the predecessor tube, the 961H, had been eliminated.

Despite extensive effort, the focusing could not be improved beyond 92% DC beam transmission and 89% with RF. However, swept RF output power was taken over a range of drive levels. Figure 17 is a plot of the saturated output power across the frequency band. As expected, the high output VSWR resulted in severe

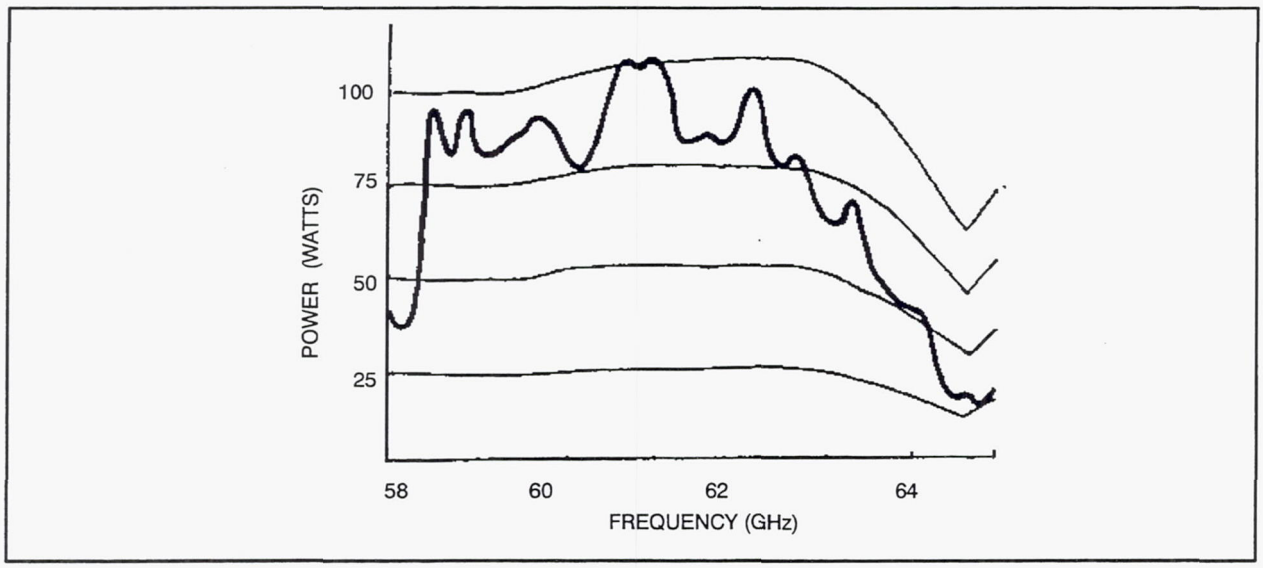

Figure 17. 961HA S/N 1 Saturated Output Power (at low duty).

gain variations across the frequency band. However, the S/N 1 results demonstrated that the passband was correct and the second harmonic interaction had been eliminated.

S/N 1 also allowed preliminary collector data to be obtained. Though the tube was only operated at 1% duty the peak output power of 100 watts at 61.5 GHz, and the calculated overall efficiency of 32% and estimated collector efficiently indicated that both the circuit and MDC designs were sound.

The first collector data were taken on the 961HA S/N 1. This tube had both poor focusing, 11% interception and a 50% VSWR in the output section. The bad match resulted in substantial gain variation. The experimental collector efficiency was calculated using the optimum frequency of 60.7 GHz; the model results are for 61.5 GHz. The measured circuit efficiency was 8% versus the predicted value of 7%. The collector efficiency was 94% and the overall efficiency 32%. Given the poor focusing and VSWR of S/N 1 the goal of 40% overall efficiency seemed achievable if the next tube had more typical focusing and matches. Table 4 summarizes the efficiency data from S/N 1.

Figure 18 shows the S/N 1 body current versus collector depression voltage, with all the stages tied together. The flat plots show that there is no backstreaming from the collector below about 15 kV depression (this fact is later used as an assumption in obtaining the estimated experimental MDC efficiency).

TABLE 4. 961HA S/N 1 EFFICIENCY DATA

Efficiency	Measured	Calculated
RF	7.95%	6.99%
Collector	93.9%	94.3%
Overall	32.2%	44.8%

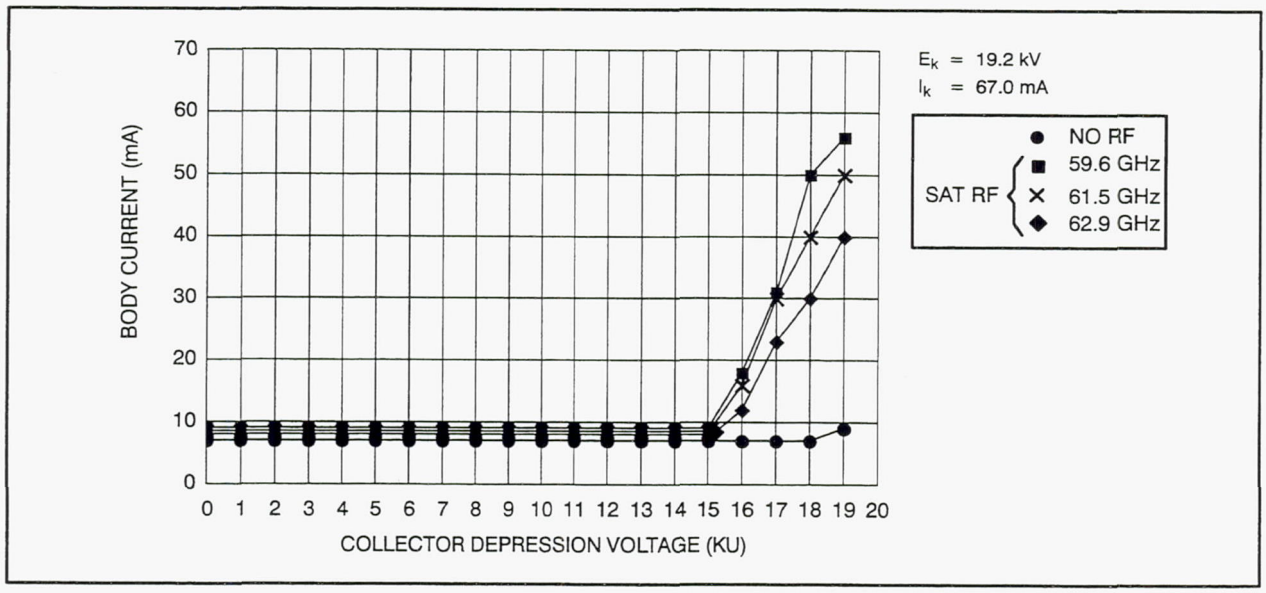

Figure 18. S/N 1 Body Current versus Collector Depression.

4.2 961HA S/N 2

After the difficulty experienced assembling S/N 1 it was decided to change to a more modern V-band coupler and window design. The output circuit had already been assembled. However the new coupler and RF window (described in Section 3.4) were installed on the input. A check of the transmission prior to the termination braze indicated only −5 dB of transmission loss, typical for these type of V-band circuits. Prior to stack braze the matches were less than 10% reflection at the input and 20% at the output. Like S/N 1, S/N 2 also experienced vacuum leaks at stack braze. Multiple attempts were required to seal the tube. The final output match was 40% and the input, 30%.

The tube was processed to test. The focusing was worse than S/N 1, only 50% DC transmission. The magnet stack was reversed with no effect. A higher strength magnet stack was tried, but did not improve the transmission. Five heat risers were removed from the bottom of the input circuit to allow shunting along the bottom. This also did not improve the focusing beyond the 50% transmission. Temperature measurement showed that the input of the circuit was the hottest and therefore the beam was intercepting at the entrance. No external misalignments, such as a bend, could be measured. The magnets were removed and the tube body x-rayed; no blockages or misalignments could be detected.

At this point an extensive failure analysis was conducted. There were two thrusts, beam optics and mechanical alignments. The beam optics study, described in detail in Section 3.2, determined that the large cathode to first magnet distance required a large input coupler magnet to focus the beam which created magnetic end effects and beam ripple. The range of mechanical tolerances were evaluated. These tolerances were compared to the predicted maximum beam size. The nominal clearance of the 961HA design was less than on a production V-band TWT. It was also found that the 961HA gun pole piece distorted after brazing. A cleanup machining after brazing was incorporated for the 961HA S/N 3. The predicted clearance of the electron beam edge, r95, to the beam hole for S/N 3 was improved from the 0.0012 in. of S/N 2 to 0.0029 in.

4.3 961HA S/N 3

S/N 3 was redesigned to address the deficiencies of the first two tubes. The electron gun was redesigned to eliminate one anode. This allowed a more optimum placement of the magnetic field with respect to the circuit. Now that the cathode could be closer to the magnetic field, a smaller weaker coupler magnet could be used at the circuit entrance. This weaker magnet eliminated rather severe end effects (variation in cell to cell magnetic field) that we believe created ripple in the beam. The gun pole piece was machined prior to final assembly for optimum alignment. To achieve a better VSWR at final assembly the output coupler was changed to monel, a stiffer material. Also this coupler was a much simpler design that required fewer braze assembly steps than the previous design. Finally the circuit vacuum assembly was built in two halves and welded together for final assembly. This allowed better control of the braze joint temperatures required to seal the circuit to the focusing structure.

The final VSWRs of the S/N 3 output and input circuits were 20%. The tube focused easily at turn-on. The initial focusing with 80 mA of cathode current was 2.5 mA DC body current, 3.1% interception. Figures 19 show the low duty output power across the frequency band for 80 and 72 mA beam current. The dashed lines indicate that the tube oscillated at those drive levels. This drive induced oscillation was at the fundamental mode upper cutoff. The oscillation mechanism is that so much power is extracted from the beam that it slows down to a velocity synchronous with the upper cutoff of the fundamental mode. The tube was restacked with a slightly higher field magnet stack to reduce the beam size, and thereby the RF wave-beam interaction, and hopefully the oscillation. This reduced the onset of the oscillation but did not eliminate it entirely. The original stack was used for best focusing. The drive-induced oscillation could be eliminated by reducing the beam current to 76 mA and selecting an input drive that did not overdrive the upper end of the frequency band.

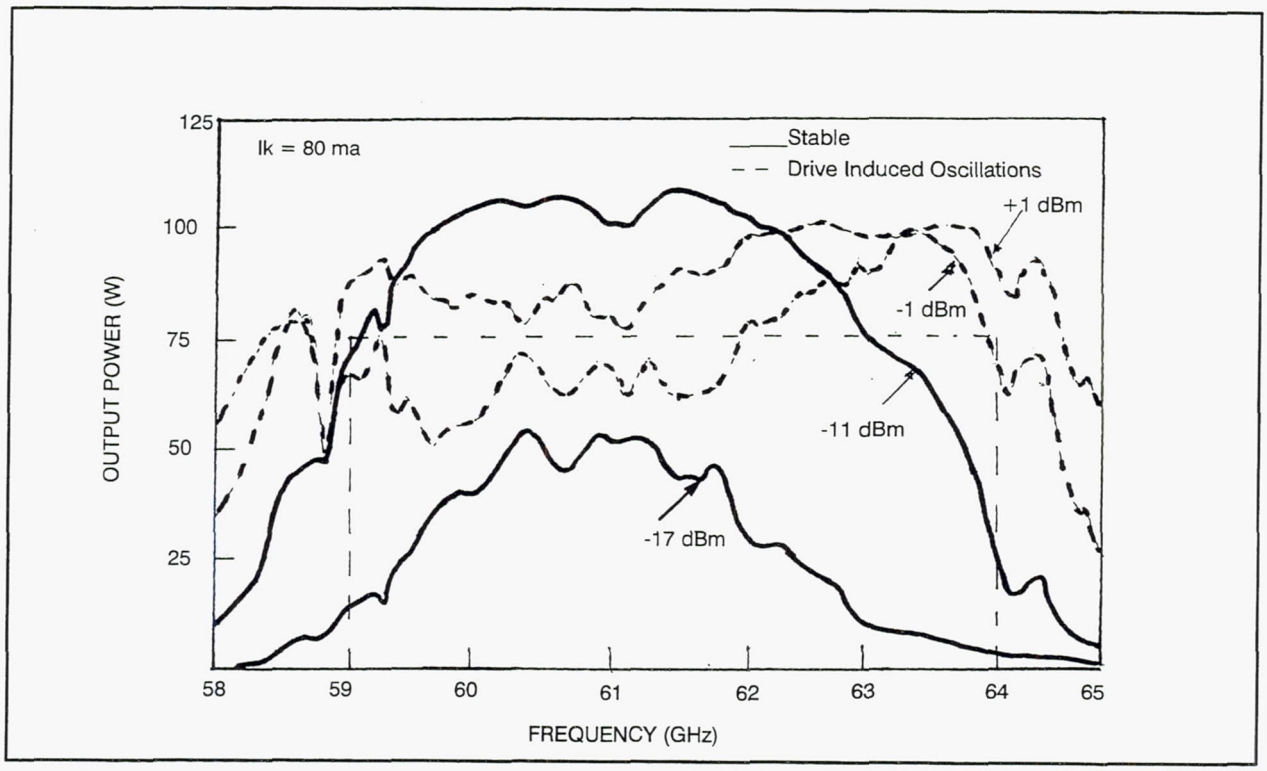

Figure 19a. 961HA S/N 3 Low Duty Swept Output Power (80 mA Beam Current).

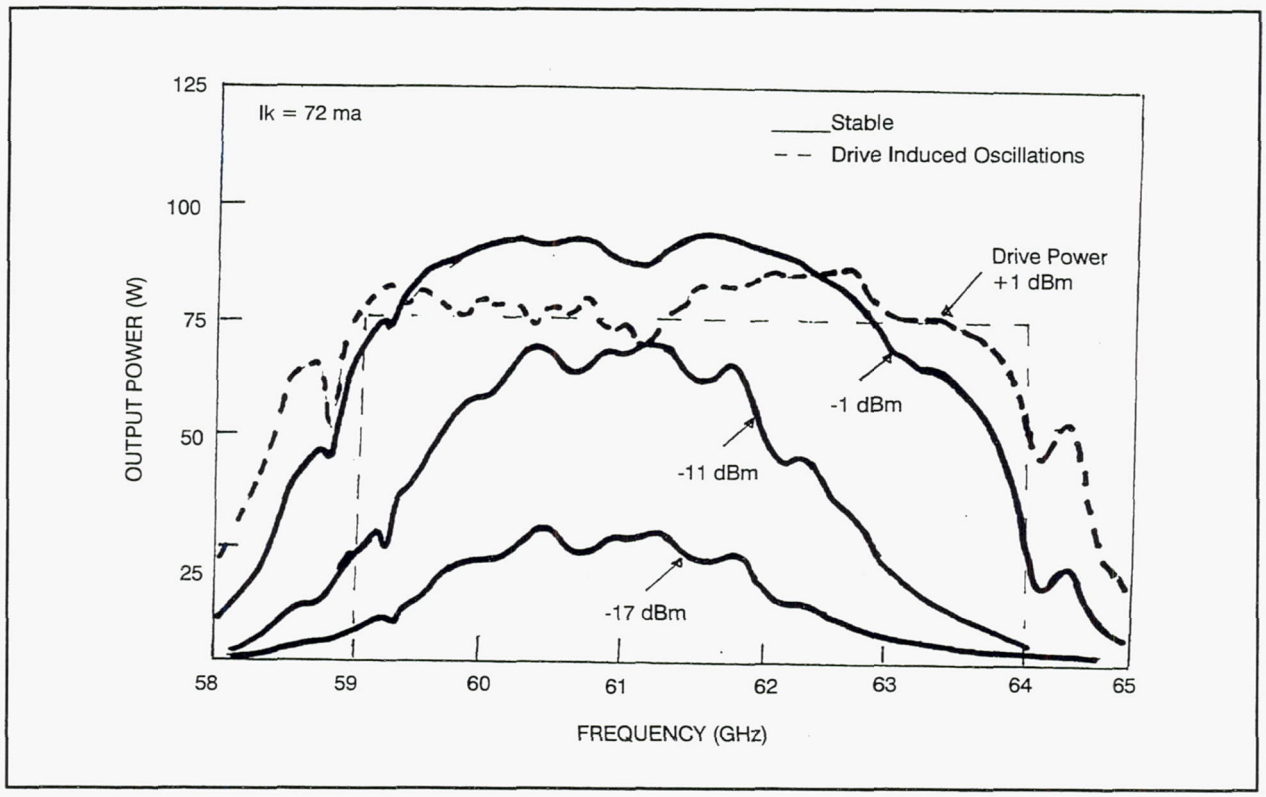

Figure 19b. 961HA S/N 3 Low Duty Swept Output Power (72 mA Beam Current.)

The tube was nameplated at 74 mA beam current and −3 dBm input drive power. The tube was processed CW at these parameters. Figure 20 is a swept plot of the CW output power versus frequency at a constant input drive power. The frequency band was further divided into smaller sections and aged at an input drive to saturate. Figure 21 is the point-by-point saturated CW output power and the estimate of output power if the output waveguide and window were copper. Please note that the tube is stable under these conditions. The small signal gain is plotted in Figure 22. The large parabolic component is expected for this bandwidth. Due to the good matches the small signal gain ripple is small for this class of tubes, less than 2 dB. The phase ripple is generally proportional to the small signal gain ripple; therefore we expect it to be less than 15° (quite good for a V-band TWT). A photograph of the completed 961HA S/N 3 TWT was shown in Figure 1. This tube has been delivered.

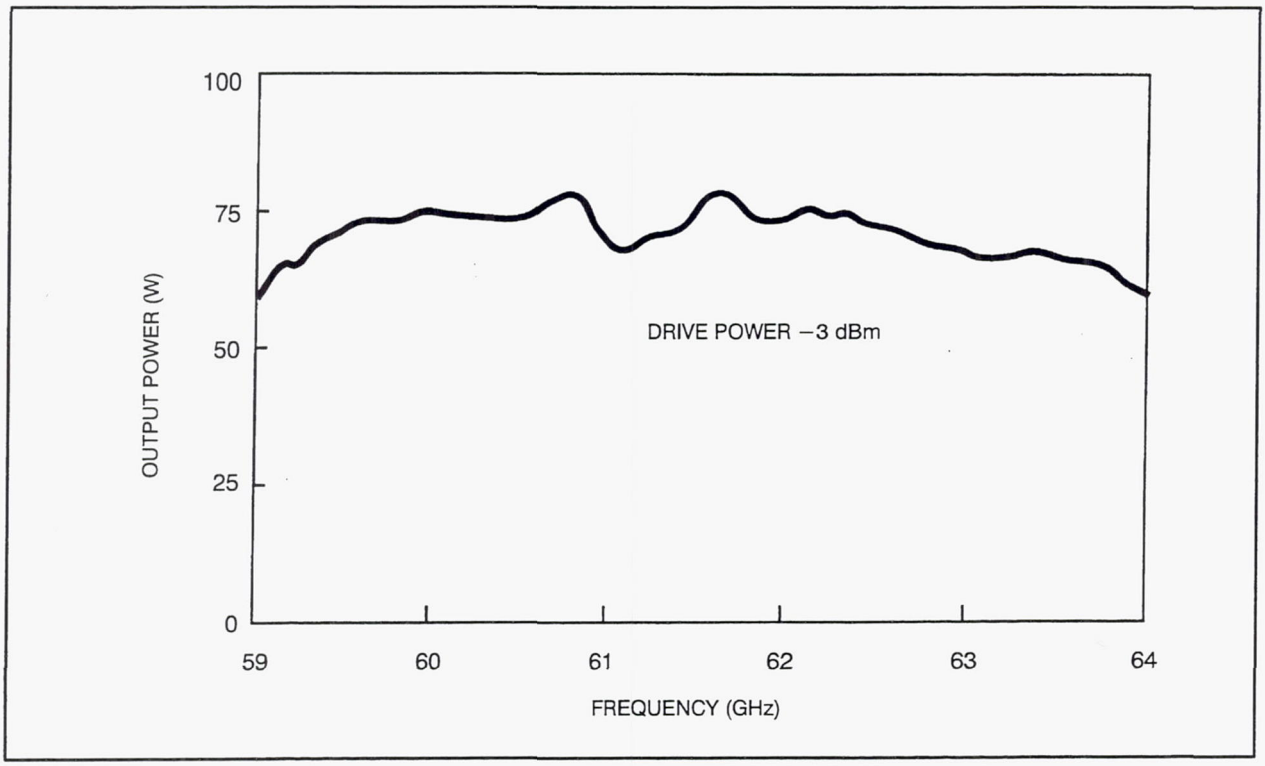

Figure 20. 961HA S/N 3 CW output power at constant drive and nameplate operating parameters.

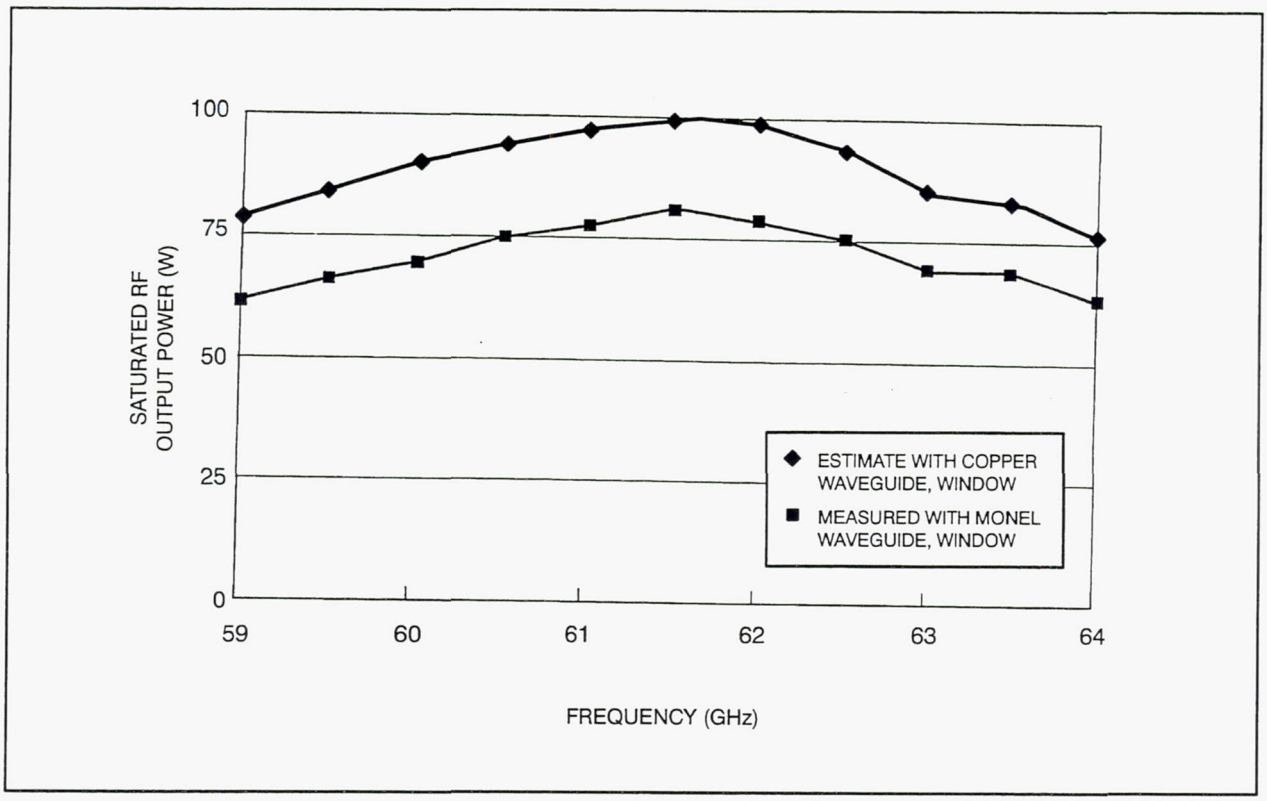

Figure 21. 961HA S/N 3 CW saturated output power at nameplate operating parameters.

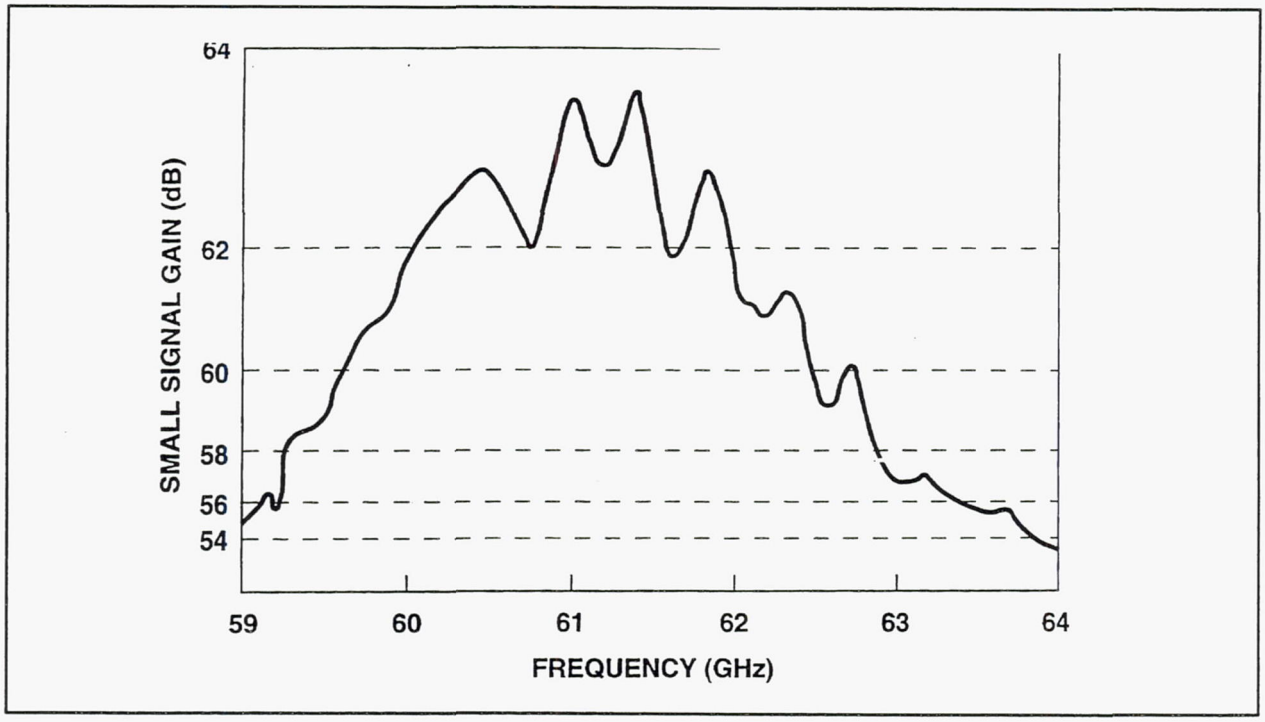

Figure 22. 961HA S/N 3 small signal gain at nameplate operating parameters.

The lossier output waveguide incorporated on S/N 3 degraded the output power an estimated 0.84 to 0.99 dB (a function of frequency). Table 5 shows the RF power losses of the output waveguide and window and of the TWT circuit. These losses substantially reduce the output power and efficiency.

TABLE 5. WAVEGUIDE, WINDOW AND TWT CIRCUIT LOSSES

Transformer Loss

Frequency (GHz)	Monel (dB)	Copper (dB)	Monel-Cu difference (dB)
59.0	1.20	0.21	0.99
61.5	1.08	0.19	0.89
61.0	1.01	0.17	0.84

Window Loss

Frequency (GHz)	Monel (dB)	Copper (dB)	Monel-Cu difference (dB)
59.0	0.73	0.13	0.060
61.5	0.70	0.12	0.058
61.0	0.68	0.12	0.056

Total Loss Difference Between Monel and Copper

Frequency (GHz)	Monel-Cu difference (dB)
59.0	1.05
61.5	0.95
61.0	0.90

Calculated TWT Circuit Losses

Frequency (GHz)	TWT Circuit Loss
59.0	14.3%
61.5	16% (Saturation) 22.7% (Overdriven)
61.0	23.5%

Table 6 shows the experimental results at saturation of S/N 3. The input power was adjusted so as to achieve maximum output power at each frequency shown. Figure 23 shows the overall efficiency versus frequency of S/N 3 as measured and also as if the output transformer and window were copper. Table 7 shows the experimental multiple stage depressed collector efficiencies versus frequency. These efficiencies were calculated after allowing for the losses shown in Table 5. Figure 24 shows the swept RF output power versus frequency with RF input power as a parameter. Table 8 shows the S/N 3 experimental results versus input power.

TABLE 6. 961HA S/N 3 EXPERIMENTAL RESULTS AT SATURATION

Freq (GHz)	E_k (kV)	E_{b1} (kV)	E_{b2} (kV)	E_{b3} (kV)	E_{b4} (kV)	I_w (mA)	I_{b1} (mA)	I_{b2} (mA)	I_{b3} (mA)	I_{b4} (mA)	I_k (mA)	P_{out} (dBm)	P_{out} (Watts)	P_{in} (dBm)	Eff (%)
59.0	19.3	14.9	16.6	18	19.3	2.9	16	38	16.9	0	73.8	47.82	60.5	−4	24.11
59.5	19.3	14.9	16.6	18	19.3	2.9	18	37	15.9	0	73.8	48.15	65.3	−4	25.53
60.0	19.3	14.9	16.6	18	19.3	2.9	19	36	15.9	0	73.8	48.39	69.0	−6	26.80
60.5	19.3	14.9	16.6	18	19.3	2.9	22	33	15.9	0	73.8	48.75	74.6	−5	28.41
61.0	19.3	14.9	16.6	18	19.3	2.9	23	30	17.9	0	73.8	48.88	77.3	−5	29.57
61.5	19.3	14.9	16.6	18	19.3	2.9	24	27	19.9	0	73.8	49.07	80.7	−7	31.00
62.0	19.3	14.9	16.6	18	19.3	2.9	24	24	22.9	0	73.8	48.97	78.9	−6	30.80
62.5	19.3	14.9	16.6	18	19.3	2.9	24	22	24.9	0	73.8	48.77	75.3	−6	29.72
63.0	19.3	14.9	16.6	18	19.3	2.9	23	20	27.9	0	73.8	48.38	68.9	−4	27.85
63.5	19.3	14.9	16.6	18	19.3	2.9	23	18	29.9	0	73.8	48.38	69.0	−2	28.20
64.0	19.3	14.9	16.6	18	19.3	2.9	22	17	31.9	0	73.8	48.02	63.4	−1	26.40

TABLE 7. EXPERIMENTAL MDC EFFICIENCIES VERSUS FREQUENCY

Frequency (GHz)	Collector Efficiency (%)
59.0	91.8
61.5	93.2
64.0	93.5
DC	92.3

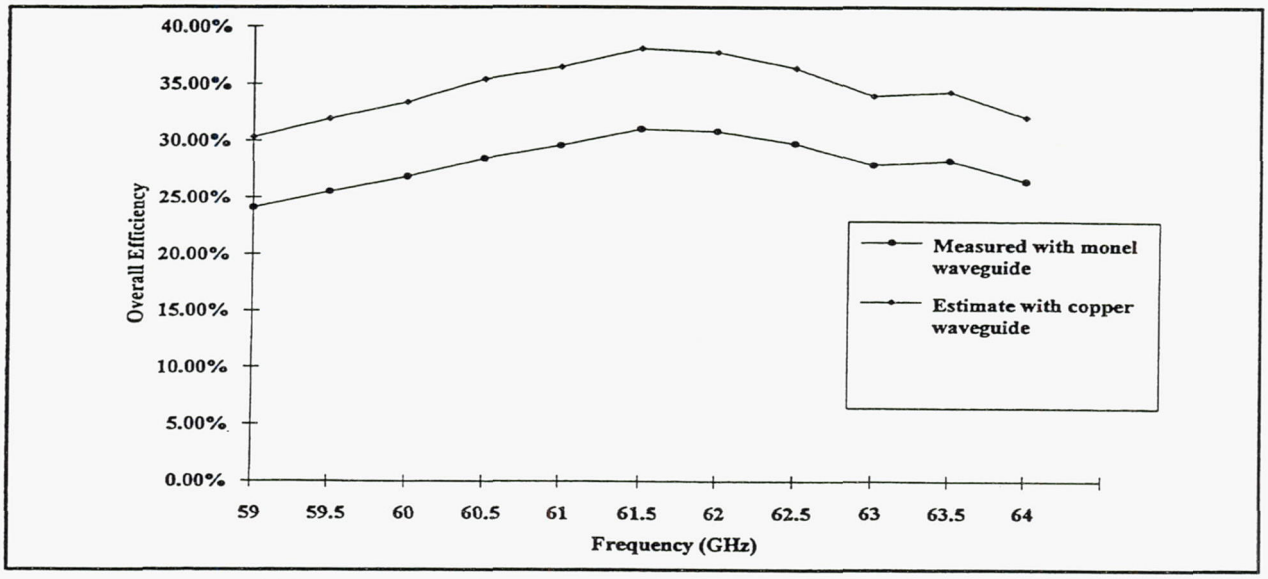

Figure 23. 961HA S/N 3 overall efficiency at nameplate beam parameters with the input drive power adjusted to saturation.

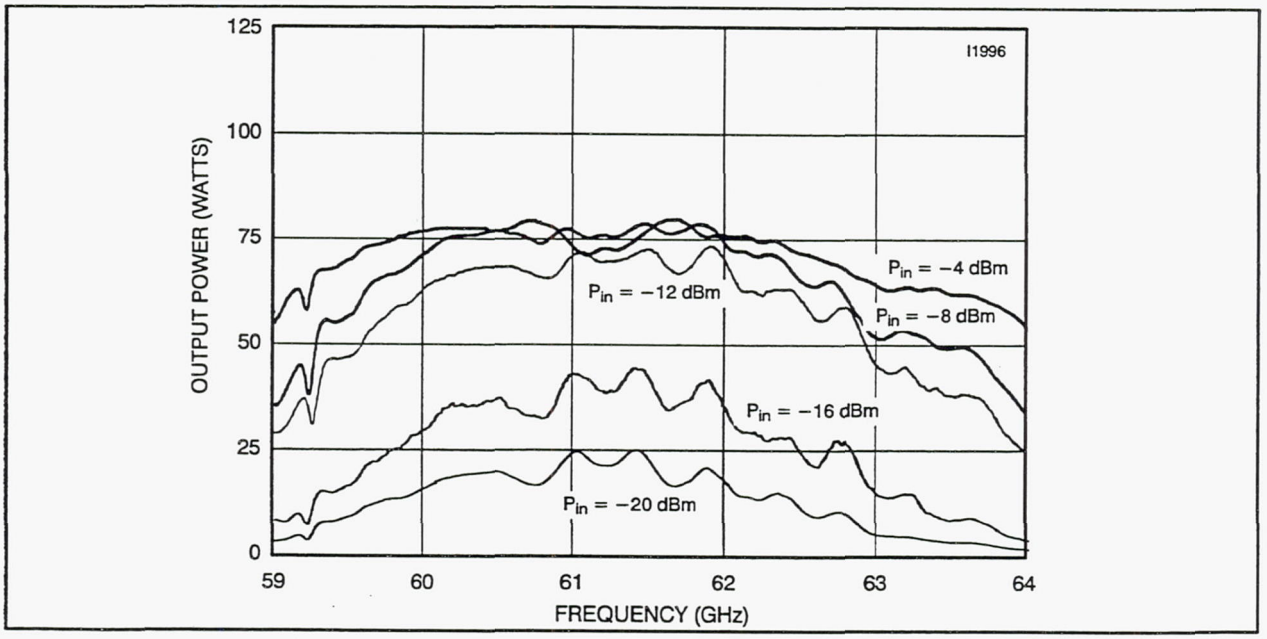

Figure 24. Swept S/N 3 RF output power with RF input power as a parameter and nameplate beam parameters.

TABLE 8. 961HA S/N 3 EXPERIMENTAL RESULTS VERSUS INPUT POWER (P_{IN})

Freq (GHz)	E_k (kV)	E_{b1} (kV)	E_{b2} (kV)	E_{b3} (kV)	E_{b4} (kV)	I_w (mA)	I_{b1} (mA)	I_{b2} (mA)	I_{b3} (mA)	I_{b4} (mA)	I_k (mA)	P_{out} (dBm)	P_{out} (Watts)	P_{in} (dBm)	Eff (%)
59	19.3	14.9	16.6	18	19.3	2.8	14	37	20.0	0	73.8	47.79	60.1	−3	24.88
59	19.3	14.9	16.6	18	19.3	2.6	7	32	32.2	0	73.8	46.37	43.4	−6	20.74
59	19.3	14.9	16.6	18	19.3	2.4	4	26	41.1	0	73.8	44.60	28.8	−9	15.32
59	19.3	14.9	16.6	18	19.3	2.1	3	19	49.7	0	73.8	42.27	16.9	−12	9.96
59	19.3	14.9	16.6	18	19.3	2.0	2	13	56.8	0	73.8	39.92	9.8	−15	6.27
61.5	19.3	14.9	16.6	18	19.3	3.0	26	23	21.8	0	73.8	48.88	77.1	−3	29.34
61.5	19.3	14.9	16.6	18	19.3	3.0	26	26	18.8	0	73.8	49.00	79.4	−6	29.74
61.5	19.3	14.9	16.6	18	19.3	2.8	25	27	19.0	0	73.8	48.87	77.1	−9	29.47
61.5	19.3	14.9	16.6	18	19.3	2.7	19	26	26.1	0	73.8	48.17	65.6	−12	27.35
61.5	19.3	14.9	16.6	18	19.3	2.4	14	23	34.4	0	73.8	46.97	49.8	−15	23.19
64	19.3	14.9	16.6	18	19.3	2.6	22	15	34.2	0	73.8	47.62	57.8	−3	24.92
64	19.3	14.9	16.6	18	19.3	2.3	18	13	40.5	0	73.8	46.97	49.8	−6	23.56
64	19.3	14.9	16.6	18	19.3	2.2	8	16	47.6	0	73.8	44.97	31.4	−9	17.18
64	19.3	14.9	16.6	18	19.3	2.1	3	14	54.7	0	73.8	41.37	13.7	−12	8.42
64	19.3	14.9	16.6	18	19.3	1.9	2	11	58.9	0	73.8	37.97	6.3	−15	4.15

5.0 CONCLUSIONS

The development of the 961HA TWT has extended the performance of V-band space TWTs in both bandwidth and output power. An average of 70 watts of CW output power was achieved from 59 to 64 GHz. The output power ranged from 60 watts at the band edges to a peak output power of 77 watts at band center. The TWT had an excellent output match, less than 20%, leading to very minimal small signal gain ripple, 2 dB. (Though the phase characteristics of this TWT were not measured, phase variation is proportional to the small signal gain variation and therefore expected to be quite good). The minimum overall efficiency was 25% at the band edges; considering the 5 GHz bandwidth of the device this is excellent.

Many challenges were encountered in the development of this TWT. The major hurdles, unexpectedly, were focusing and assembly technique. It was not until S/N 3 that acceptable focusing and RF matches were obtained, that the issues of bandwidth, output power, and efficiency could be addressed. Some conclusions and recommendations can be made for future devices of this type.

1. Possible end effects due to the coupler magnet need to be included in the gun design model.
2. The split focusing structure assembly technique, employed on S/N 3, is recommended for millimeter-wave PPM focused TWTs. This technique involves building the TWT vacuum assembly in two halves. This provides more accurate control of the critical focusing structure-to-circuit vacuum seal, resulting in improved VSWRs and vacuum assembly yield. It also allows the circuits to be independently repaired or replaced.
3. For V-band reentrant ferruled coupled cavity RF circuits to avoid stability problems, 35% cold bandwidth is the practical upper limit. At lower frequencies selective loss is introduced to overcome this limitation, but is not mechanically practical at V-band dimensions.
4. Beam interception can be reduced by perhaps 30% by enlarging the inner diameter of the adjustable ferrules at the input. This is now being done on new designs of other millimeter-wave TWTs at Hughes (but they have not yet been tested as of this date). Combined with 25% more RF interaction efficiency obtainable from using copper output transformers and windows, better focusing would make the 40% overall efficiency goal achievable.
5. Future design efforts need to concentrate on developing a rugged low loss coupler; an estimated 0.9 to 1.16 dB of output power is lost in the current output coupler design. The output power and efficiency goals of 75 watts and 40% efficiency could then be achieved without pushing the circuit into oscillation.

6.0 REFERENCES

1. A. L Rousseau, I. Tammaru, and J. P. Vaszari, "Development of a 75 Watt 60 GHz Traveling-Wave Tube for Intersatellite communications," NASA CR-182135, 1988.

2. Jeffrey D. Wilson., Peter Ramins, Dale A. Force, Helen C. Limburg, and Ivo Tammaru, "A High-Efficiency 59- to 64-GHz TWT for Intersatellite Communications", IEDM 1991 pp. 585-588.

3. Jeffrey D. Wilson, Peter Ramins, and Dale A. Force, "Spent-Beam Defocusing Analysis and Multistage Depressed Collector Design for a 75-W 59- to 64-GHz Coupled Cavity TWT." NASA TP3039, 1990.